Science Translational Medicine AAAS

Submitted Manuscript: Confidential template updated: February 28 2012

Supplementary Material for

Glycine-based treatment ameliorates NAFLD by modulating fatty acid oxidation, glutathione synthesis, and the gut microbiome

Oren Rom[1*], Yuhao Liu[1], Zhipeng Liu[2], Ying Zhao[1], Jianfeng Wu[3], Alia Ghrayeb[4], Luis Villacorta[1], Yanbo Fan[5], Lin Chang[1], Lu Wang[6], Cai Liu[6], Dongshan Yang[7], Jun Song[7], Jason C. Rech[8], Yanhong Guo[1], Huilun Wang[1], Guizhen Zhao[1], Wenying Liang[1], Yui Koike[1], Haocheng Lu[1], Tomonari Koike[1], Tony Hayek[9,10], Subramaniam Pennathur[1], Chuanwu Xi[3], Bo Wen[6], Duxin Sun[6], Minerva T. Garcia-Barrio[1], Michael Aviram[9], Eyal Gottlieb[4], Inbal Mor[4], Wanqing Liu[11], Jifeng Zhang[1], and Y. Eugene Chen[1,7*]

*Corresponding author. Email: echenum@umich.edu (Y.E.C.); roren@umich.edu (O.R.)

Materials and Methods

Histology and immunohistochemistry

All histological procedures were performed by technicians at the University of Michigan (U-M) In Vivo Animal Core (IVAC) Histology Laboratory. Technicians were blinded to experimental groups. Formalin-fixed tissues were processed through graded alcohols and cleared with xylene followed by infiltration with molten paraffin using an automated VIP5 or VIP6 tissue processor (TissueTek, Sakura-Americas). Using a Histostar Embedding Station (ThermoFisher Scientific), tissues were then sectioned on a M355S rotary microtome (ThermoFisher Scientific) at 4 µm thickness and mounted on glass slides. Slides were stained for hematoxylin and eosin (H&E, ThermoFisher Scientific). For Sirius Red staining, slides were treated with 0.2 phosphomolybdic acid for 3 min and transferred to 0.1% Sirius Red saturated in picric acid (Rowley Biochemical Inc.) for 90 min, then transferred to 0.01N hydrochloric acid for 3 min.

Frozen section processing was used for Oil Red O (ORO) staining. Formalin-fixed liver samples were cryoprotected in 20% sucrose at 4^{o}C overnight, blotted, then liquid nitrogen-snap frozen in OCT compound (Tissue-Tek) and stored at -80^{o}C until ready for cryosectioning. Prior to sectioning, frozen blocks were brought up to about -20^{o}C, then sectioned at 5 µm on a Cryotome SME (Thermo-Shandon). Slides were stored at -80^{o}C until stained. Prior to staining, liver slides were thawed to room temperature for 30 min. Slides were post-fixed in 10% Neutral Buffered Formalin for 20 min, rinsed in DDW, followed by rinsing in 60% isopropanol before being placed in working ORO-isopropanol stain (Rowley Biochemical Inc., H-503-1B) for 5 min. Slides were then rinsed in 60% isopropanol followed by three changes of DDW. Then, slides were nuclear counterstained in Harris Hematoxylin and mounted in Aqua-Mount (Lerner Laboratories) aqueous mounting media.

Immunohistochemical staining was performed on a IntelliPATH FLX automated immunohistochemical stainer (Biocare Medical) with blocking for endogenous peroxidases and non-specific binding, followed by detection using a horseradish peroxidase biotin-free polymer based commercial detection system, disclosure with diaminobenzidine chromogen, and nuclear counterstaining with hematoxylin. Specific to F4/80, (Bio-Rad ABD Serotec), the rat monoclonal primary antibody (clone CI:A3-1) was diluted to 1:400 in DaVinci Diluent (Biocare Medical) and incubated for 60 min followed by detection using Rat-on-Mouse HRP-Polymer, (Biocare Medical) 2-step probe-polymer incubation for 10 and 30 min respectively.

NAFLD activity and fibrosis scores

H&E staining was used to score NAS (*3, 25*). Steatosis was scored from 0-3 (0: <5% steatosis; 1: 5-33%; 2: 34-66%; 3: >67%). Hepatocyte ballooning was scored from 0-2 (0: normal hepatocytes, 1: normal-sized with pale cytoplasm, 2: pale and enlarged hepatocytes, at least 2-fold). Lobular inflammation was scored from 0-2 based on foci of inflammation counted at 20X (0: none, 1: <2 foci; 2: ≥2 foci). NAS was calculated as the sum of steatosis, hepatocyte ballooning and lobular inflammation scores. Sirius Red staining was used to score hepatic fibrosis from 0-4 (0: no fibrosis; 1: perisinusoidal or portal fibrosis; 2: perisinusoidal and portal fibrosis; 3: bridging fibrosis; 4: cirrhosis).

Plasma analyses

Complete plasma lipid profile (TC, TG, LDL and HDL) was measured with a Cobas Mira chemistry analyzer (Roche Diagnostics) at the Chemistry Laboratory of the Michigan Diabetes Research Center (MDRC) using manufacturer-provided reagents or protocols at our lab, using commercially available kits (Wako Diagnostics). Plasma leptin and resistin were measured on a Luminex 200 platform (Luminex) at the MDRC using a Multiplex Assay (Millipore). Plasma MCP-1 was measured with the mouse CCL2/JE/MCP-1 Quantikine ELISA Kit (R&D Systems). Clinical chemistry assays for ALT, AST and ALP were performed by the University of Michigan IVAC on a Liasys 330 chemistry analyzer (AMS Diagnostics) using manufacturer-provided reagents and protocols. Plasma oxalate was measured using Abcam's oxalate assay kit. Plasma glucose was measured using glucometer and test strips (Contour Next). Plasma amino acid (AA) analysis was performed by University of Michigan Metabolomics Core. Twenty µL of plasma were derivatized and prepared for GC-MS analysis according to the instructions of the EZ Faast Amino Acids Analysis kit (Phenomenex). Samples were subjected to column clean-up and transferred to a GC autosampler vial. Then, samples were derivatized, dried under a gentle nitrogen stream at room temperature, and re-suspended for GC analysis on an Agilent 69890N GC-5975 MS detector with the following parameters: 1 µL sample was injected with a 1:15 split ratio on an ZB-AAA 10m column (Phenomenex) with He gas flow rate of 1.1 mL/min. The GC oven initial temperature was 110°C and was increased by 30°C per minute to 320°C. The inlet temperature was 250°C and the MS-source and quad temperatures were 230° and 150°C respectively. Data were processed using MassHunter Quantitative analysis version B.07.00. Metabolites were normalized to the nearest isotope labeled internal standard and quantified using 2 replicated injections of 5 standards to create a linear calibration curve with accuracy better than 80% for each standard. Peak areas were used for differential analysis between groups.

Liver analyses

Livers were rapidly removed from the euthanized mice, snap-frozen in liquid nitrogen, and kept at -80°C. Frozen liver samples (100 mg) were homogenized in PBS and centrifuged (14,000 RPM, 20 min). The supernatants were collected and analyzed for protein concentration using Bio-Rad Bradford assay. To assess liver lipid composition, lipids were extracted from the supernatants using hexane (≥99%, Sigma-Aldrich) and isopropanol (≥99.5%, Fisher Scientific) at a 3:2 ratio (v:v), and the hexane phase was left to evaporate for 48 h (*25*, *60*). The amount of liver TG or TC was determined spectrophotometrically using commercially available kits (Wako Diagnostics). Liver DAG and MDA were determined using an ELISA kit (Aviva Systems Biology) and Cayman's TBARS assay kit, respectively, according to the manufacturers' instructions. Hepatic TG, TC, DAG and MDA data were normalized to protein concentrations. Liver DT-109 and GSH were assessed using LC-MS/MS as detailed below.

Body composition and comprehensive laboratory animal monitoring system (CLAMS)

All measurements were performed by technicians at the U-M Animal Phenotyping Core. Body fat, lean body mass, and free fluids were measured using a nuclear magnetic resonance (NMR)-based analyzer (Minispec LF90II; Bruker Optics). The analyzer is daily checked using a reference sample as recommended by the manufacture. The mice were placed individually into

the measuring tube with minimum restrain. Oxygen consumption (VO_2), carbon dioxide production (VCO_2) and motor activity were measured using CLAMS (Columbus Instruments), an integrated open-circuit calorimeter equipped with an optical beam activity monitoring device. Mice were weighed before the measurements and individually placed into the sealed chambers (7.9" x 4" x 5") with free access to food and water. The study was carried out in an experimentation room set at 20-23°C with 12-12 h dark-light cycles (6:00PM-6:00AM). Measurements were carried out continuously for 48 h. During this time, animals were provided with food and water through the feeding and drinking devices located inside the chamber. VO_2 and VCO_2 in each chamber were sampled sequentially for 5s in 10 min intervals and the motor activity was recorded every second in X and Z dimensions. The air flow rate through the chambers was adjusted to keep the oxygen differential around 0.3% at resting conditions. Respiratory exchange ratio (RER) was calculated as VCO_2/VO_2. Total energy expenditure, glucose oxidation and fat oxidation were calculated based on the values of VO_2, VCO_2, and the protein breakdown.

Identification of glycine-based compounds

Compounds structurally similar to glycine were chosen to evaluate structural, conformational, electrostatic or isosteric modifications to the glycine scaffold (Fig. S7A). Searches were conducted via SciFinder to determine commercial availability. N-methylglycine (Fig. S7B), N,N-dimethylglycine (Fig. S7C), and N,N,N-trimethylglycine (Fig. S7D) explored various degrees of methylation on the glycine amine moiety, while glycolic acid (Fig. S7E) evaluated an amine to alcohol substitution. Modifications to the acid region were explored by glycinamide (Fig. S7F), 2-amino-N-methylacetamide (Fig. S7G), and ethanolamine (Fig. S7H), while 2-oxopiperazine (Fig. S7I) and morpholin-2-one (Fig. S7J) explored conformationally restricted analogues. (1H-tetrazol-5-yl) methanamine (Fig. S7K) explored the isosteric replacement of the acid. Water-soluble compounds with oral LD_{50}>1 mg/g were defined as suitable for oral administration to mice.

Oral glucose tolerance tests (OGTT)

OGTT were performed after 12 h fasting. Blood samples were taken from the tail tip at 0, 15, 30, 60 and 120 min after oral gavage of glucose (2 mg/g body weight) with or without leucine, glycine, DT-109 or other glycine-based compounds at the indicated dosages. Blood glucose concentrations were measured using a glucometer and test strips (Contour Next).

RNA-Sequencing and data analysis

Total RNA from mouse liver samples was extracted using QIAGEN's RNeasy kit (QIAGEN). Library preparation and sequencing were performed by the U-M DNA Sequencing Core. RNA was assessed for quality using the TapeStation (Agilent, Santa Clara, CA). All samples had RNA integrity numbers (RINs) >8.5. Samples were prepared using the NEBNext Ultra II Directional RNA Library Prep Kit for Illumina (NEB) with Poly(A) mRNA Magnetic Isolation Module (NEB) and NEBNext Multiplex Oligos for Illumina Unique dual (NEB), where 10 ng - 1 µg of total RNA were subjected to mRNA polyA purification. The mRNA was then fragmented and copied into first strand cDNA using reverse transcriptase and dUTP mix.

Samples underwent end repair and dA-Tailing step followed by ligation of NEBNext adapters. The products were purified and enriched by PCR to create the final cDNA library. Final libraries were checked for quality and quantity by TapeStation (Agilent) and qPCR using Kapa's library quantification kit for Illumina Sequencing platforms (Kapa Biosystems). Libraries were paired-end sequenced on a NovaSeq 6000 Sequencing System (Illumina).

The quality of the raw FASTQ files was checked through FastQC v0.11.8 (https://www.bioinformatics.babraham.ac.uk/projects/fastqc/). Trimmomatic v.0.35 was used to trim the low-quality reads with the parameters: SLIDINGWINDOW:4:20 MINLEN:25 (*61*). The resulted high-quality reads were then mapped to the mouse reference genome (GRCm38.90) using HISAT2 v.2.1.0.13. Gene expression quantification was performed using HTSeq-counts v0.6.0 based on the GRCm38.90 genome annotations (*62*). The R package DESeq2 was then used to identify significant differentially expressed genes (DEG) (*63*). We considered genes with adjusted *P* value less than 0.05 and absolute fold change larger than 2 as significant DEG. The up- and down-regulated DEGs were then analyzed respectively for significantly enriched KEGG pathways using the clusterProfiler package (*64*). The significance of the enrichment was determined by right-tailed Fisher's exact test followed by Benjamini-Hochberg multiple testing adjustment.

Quantitative real-time PCR analysis

Total RNA from mouse liver samples was extracted using QIAGEN's RNeasy kit (QIAGEN). RNA was reverse-transcribed into cDNA with SuperScript III and random primers (Invitrogen). Specific transcript was assessed by a real-time PCR system (Bio-Rad) using iQ SYBR Green Supermix (Bio-Rad) and the ΔΔCt threshold cycle method of normalization. Gene expression was normalized to *Gapdh*. Primer pairs used for qPCR were obtained from Integrated DNA Technologies and are listed in table S3.

Western blot analysis

Liver samples were lysed in radioimmunoprecipitation assay buffer (Thermo Scientific) supplemented with a protease/phosphatase inhibitor cocktail (Roche Applied Science). Proteins were resolved in 10% SDS-PAGE and transferred to nitrocellulose membranes (Bio-Rad). The membranes were incubated with the following primary antibodies at 4°C overnight: AGXT1 (Santa Cruz Biotechnology, 1:500), HADHA (Proteintech, 1:1000), HADHB (ABclonal, 1:1000), ACAA2 (ABclonal, 1:500), phospho-SMAD2 (Ser465/467, Cell Signaling, 1:1000), SMAD2 (Cell Signaling Technology, 1:1000), GAPDH (Santa Cruz Biotechnology, 1:2000), or β-Actin (Cell Signaling Technology, 1:2000). IRDye-conjugated secondary antibodies (LI-COR Biosciences, 1:10000) were used. Bands were visualized and quantified using an Odyssey Infrared Imaging System (LI-COR Biosciences, version 2.1).

Fecal microbiome analysis

Fecal DNA extraction, amplification using primers specific to the V4 region of the 16S rRNA, characterization of the gut microbiome using LEfSe and analysis of correlations with disease parameters were performed as previously described (*65, 66*). Total genomic DNA of the

gut microbiome was extracted from fecal samples using the QIAamp DNA Stool Mini Kit (QIAGEN) according to the manufacturer's instructions. To prepare DNA for community analysis, barcoded dual-index primers specific to the V4 region of the 16S rRNA gene were used to amplify the DNA. PCR reactions comprised 5 μL of 4 μM equimolar primer set, 0.15 μL of AccuPrime Taq DNA High Fidelity Polymerase, 2 μL of 10 x AccuPrime PCR Buffer II (Thermo Fisher Scientific), 11.85 μL of PCR-grade water, and 1 μL of DNA template. The PCR conditions were 2 min at 95°C, followed by 30 cycles of 95°C for 20 s, 55°C for 15 s, and 72°C for 5 min, followed by 72°C for 10 min. Each PCR reaction was normalized using the SequalPrep Normalization Plate Kit (Thermo Fisher Scientific). The normalized reactions were pooled and quantified using the Kapa Biosystems Library qPCR MasterMix (ROX Low) quantification kit for Illumina platforms. The Agilent Bioanalyzer was used to confirm the size of the amplicon library (~399 bp) using a high-sensitive DNA analysis kit (Agilent). Pooled amplicon library was then sequenced on the Illumina MiSeq NANO platform (Microbial Systems Molecular Biology Laboratory, U-M) according to standard protocols.

DNA sequencing data was processed using Mothur according to SOP and focused primarily on α - and β - diversity based analyses (*67*). The sequences were trimmed to remove primers and barcodes, quality filtered, and chimera checked as previously described (*66*). A total of 3565 sequences in each sample were used for further statistical analysis. The trimmed DNA sequences were clustered using the average neighbor approach to form operational taxonomic units (OTUs) at 97% sequence similarity cutoff (3% sequence divergence) (*68*). Phylogenetic trees were constructed using the Clearcut program (*69*). A heatmap of the relative abundance of each OTU across all samples was generated using log2 scaling of the relative abundance values of the top 107 OTUs (>1% abundance). Molecular AMOVA statistical analysis was performed to determine significance of structural similarity among communities across sampling groups (*70*). The UniFrac analysis was used to estimate weighted (WUnF) and unweighted (UWUnF) UniFrac metrics (*71*). Constrained ordination RDA (redundancy analysis) was calculated and the significance of environmental variables was checked by forward selection analysis (*72*). The characterization of microorganismal features differentiating the gut microbiome was performed using the linear discriminant analysis (LDA) effect size (LEfSe) method (http://huttenhower.sph.harvard.edu/lefse/) for biomarker discovery, which emphasizes both statistical significance and biological relevance (*73*). The principal component analysis (PCA) was plotted accordingly using Phyloseq package in R (*74*), where each dot represents the microbiome from fecal samples collected from one cage. The correlations between changes in the altered bacterial genera and NAFLD-related parameters in the liver or plasma were calculated using nonparametric Spearman's test. For the microbiome studies, n represents the number of cages from each experimental group. At least 3 independent cages per group were analyzed.

In vitro studies

The HepG2 human hepatoma cell line was obtained from the American Type Culture Collection (ATCC) and cultured at 37˚C and 5% CO_2 in Dulbecco's Modified Eagle Medium (DMEM, Gibco) supplemented with 10% fetal bovine serum (FBS, Sigma-Aldrich) and 1% Penicillin-Streptomycin (Pen-Strep, Gibco). In some experiments, the cells were loaded with palmitic acid (PA, 200 μM, Sigma-Aldrich) with 0.1% BSA in DMEM without FBS. siRNA targeting *AGXT1* (siAGXT1: GCAAGGAUAUGUACCAGAUtt, siRNA ID s1190) and non-

targeting siRNA control (siCTL, siRNA ID AM4611) were obtained from Ambion. HepG2 cells were transfected with 20 nM of siAGXT1 or siCTL using Lipofectamine RNAiMAX (Invitrogen) in Opti-MEM reduced-serum medium (Gibco) in accordance with the manufacturer's protocol. Cells were also transfected with a GFP-tagged human AGXT1 plasmid (OriGene, NM_000030) or control GFP plasmid using Lipofectamine 3000 (Invitrogen) in Opti-MEM reduced-serum medium (Gibco) in accordance with the manufacturer's protocol. RNA isolation, protein or lipid extraction were performed 48 h post transfection. Total RNA was purified from HepG2 cells using the QIAGEN's RNeasy kit (QIAGEN). qPCR analysis was performed using the primer pairs listed in table S3. Cells were lysed using radioimmunoprecipitation assay buffer (Thermo Scientific) supplemented with a protease/phosphatase inhibitor cocktail (Roche Applied Science). AGXT1 protein abundance was assessed using WB. Extraction of cellular lipids from the cells was done using hexane:isopropanol at a 3:2 ratio and the hexane phase was left to evaporate for 48 h. The remaining cells in the plates were disrupted in 0.1 M NaOH for 24 h and an aliquot was taken for measurement of cellular protein using the Bradford protein assay (Bio-Rad). The content of cellular TG was determined spectrophotometrically using a commercially available kit (Wako Diagnostics). Cellular TG data were normalized to protein concentrations. Oxygen consumption rate (OCR) and dependency on fatty acid β-oxidation (FAO) were assessed using a Seahorse XFe96 Analyzer (Agilent). HepG2 cells were seeded ($2.5x10^4$ cells/well) in XF96 cell culture microplates (Agilent). The next day, cells were treated with or without 1 mM DT-109 for 24 h. XFe96 sensor cartridges were hydrated in accordance with the manufacturer's instructions. Etomoxir (Agilent) and rotenone+antimycin A (R/A, Agilent) were used at final concentrations of 6 μM and 0.5 μM, respectively. OCR data were normalized to protein concentrations.

LC-MS/MS analyses of liver DT-109 and GSH

Liver samples were suspended in 20% acetonitrile-water at 1:5 (w:v) and then homogenized 8 times for 20 s each at 6500 rpm in a Precellys Evolution system. To precipitate liver proteins, 180 μL of methanol containing 25 nM internal standard (CE302) and 30 μL of methanol were added to 30 μL of homogenized liver samples and the mixture was vortexed for 10 min. The extracts were centrifuged at 3500 rpm for 10 min at 4°C, and the supernatant was transferred to the autosampler vials for LC–MS/MS analysis. For GSH determination, the extracts were centrifuged after protein precipitation as above and 200 μL of supernatant were transferred to a 96-well plate. The supernatant was evaporated using a vacuum concentrator (SpeedVac DNA 130) for 4 h at 35°C. The dry extracts were reconstituted in 80 μL H_2O, vortexed for 10 min and centrifuged at 3500 rpm for 10 min at 4°C. The supernatant was transferred to the autosampler vials for LC–MS/MS analysis. The LC–MS/MS method consisted of a Shimadzu LC-20AD HPLC system, and chromatographic separation of the DT-109 was achieved using a Waters XBridage reverse phase C18 column (5 cm x 2.1 mm I.D., packed with 3.5 μm) at 25°C. Five μL of the supernatant were injected. The flow rate of gradient elution was 0.4 mL/min with mobile phase A (0.1% formic acid in purified deionized water) and mobile phase B (0.1% formic acid in acetonitrile). An AB Sciex QTrap 4500 mass spectrometer equipped with an electrospray ionization source (ABI-Sciex) in the positive-ion multiple reaction monitoring (MRM) mode was used for detection. Protonated molecular ions and its respective ion products were monitored at the transitions of m/z 246.2 > 132.1 for DT-109 and 455.2 > 425.2 for the internal standard. For GSH analysis, Agilent Poroshell 120 EC-C18 column (50

mm x 2.1 mm I.D., 2.7 µm) and gradient elution with a low flow rate of 0.3 mL/min was used. The gradient program for mobile phase A (0.75mM Ammonium formate and 0.05% formic acid in purified deionized water) and mobile phase B (0.1% formic acid in methanol) was as follow: 0.0-3.5 min, 1% B; 3.5-4.0 min, 1-95% B; 4.0-4.5 min, 95-99% B; 4.5-4.6 min, 99-1% B; 4.6-7.6min, 1% B. Ten µL of the supernatant were injected. Protonated molecular ions and its respective ion products were monitored at the transitions of m/z 308.5 > 76.0 for GSH and 455.2 > 425.2 for the internal standard. Data were processed with software Analyst (version 1.6).

Carbon tracing and metabolomics analysis

AML-12 cells were obtained from the ATCC and cultured according to the recommendations in DMEM:F12 media (Biological Industries, Beit HaEmek, Israel) with 10% FBS supplemented with 100 U/mL penicillin, 100 µg/mL streptomycin, 40 ng/mL dexamethasone, ITSX (Gibco, 1:100) and 2 mM Glutamine (Biological Industries). For the metabolomics studies, cells were cultured in EBSS (Biological Industries) with 10% FBS supplemented with 100 U/mL penicillin, 100 µg/mL streptomycin, non-essential AA (Biological Industries 1:50) vitamins (1:50), 0.25 mM L-serine, 17 mM glucose, 2 mM glutamine, 1 mM sodium pyruvate, 1:100 ITS-X and 40 ng/mL dexamethasone. Prior to flux analyses, the cells were incubated overnight with EBSS with 1% FBS, 10 mM glucose, 1 µg/mL glutathione (Sigma-Aldrich), 0.3 ng/mL ammonium metavanadate (Sigma-Aldrich), 0.25 nM manganese chloride (Sigma-Aldrich), 2.5 mg/L ascorbic acid and 1 mM glutamine. The medium was replaced the following day with fresh metabolic medium containing 1 mM U-^{13}C labeled glutamine (Cambridge Isotope Laboratories Inc.) for 5 h in the presence or absence of glycine or DT-109 (1 mM). Metabolite extraction from the cells and LC-MS analysis were performed as previously described (*75*). TraceFinder 4.1 was used for analysis. Peak areas of metabolites were determined using the exact mass of the singly charged ions. The retention time of metabolites was predetermined on the pHILIC column by analyzing an in-house mass spectrometry metabolite library consisting of commercially available standards. For data normalization, raw data files were processed with Compound Discoverer 3.0 to obtain total compounds peak area for each sample. Each metabolite peak area value was normalized to total measurable ions in the sample. Data was visualized using Metabolite Autoplotter.

Supplementary Figures

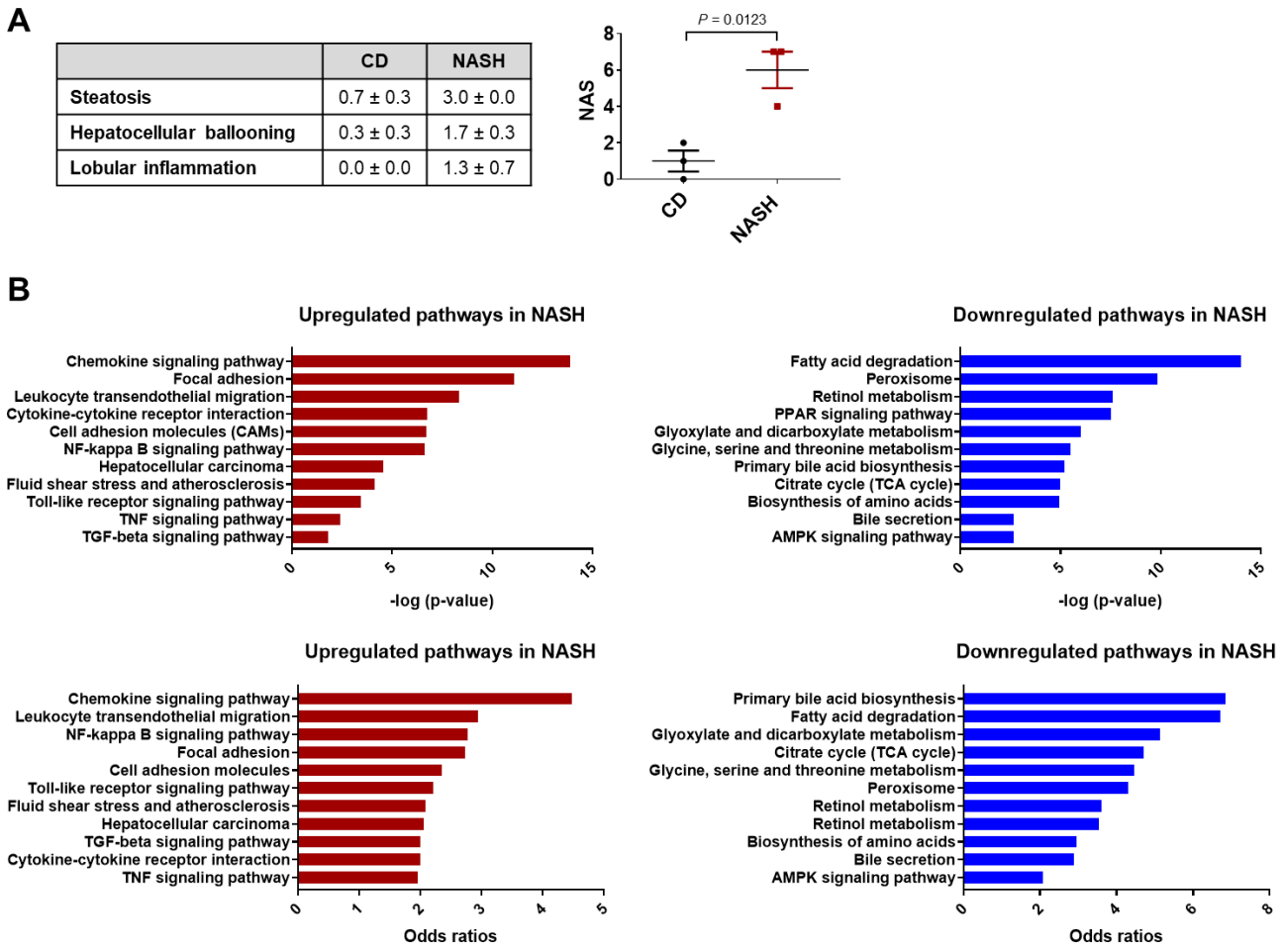

Fig. S1. Pathway analysis of livers from mice with NASH. C57BL/6J mice were fed CD or NASH-diet for 24 weeks (n=3). (A) H&E-based scoring of steatosis, hepatocellular ballooning, lobular inflammation and NAFLD activity score (NAS). Data are means ± SEM. Statistical differences were compared using Student's t test. (B) Pathway analysis following RNA-sequencing of livers. Pathways enriched in the upregulated DEG are plotted in red, while pathways enriched in the down-regulated DEG are plotted in blue. The significance of the enrichment was determined by right-tailed Fisher's exact test followed by Benjamini-Hochberg multiple testing adjustment.

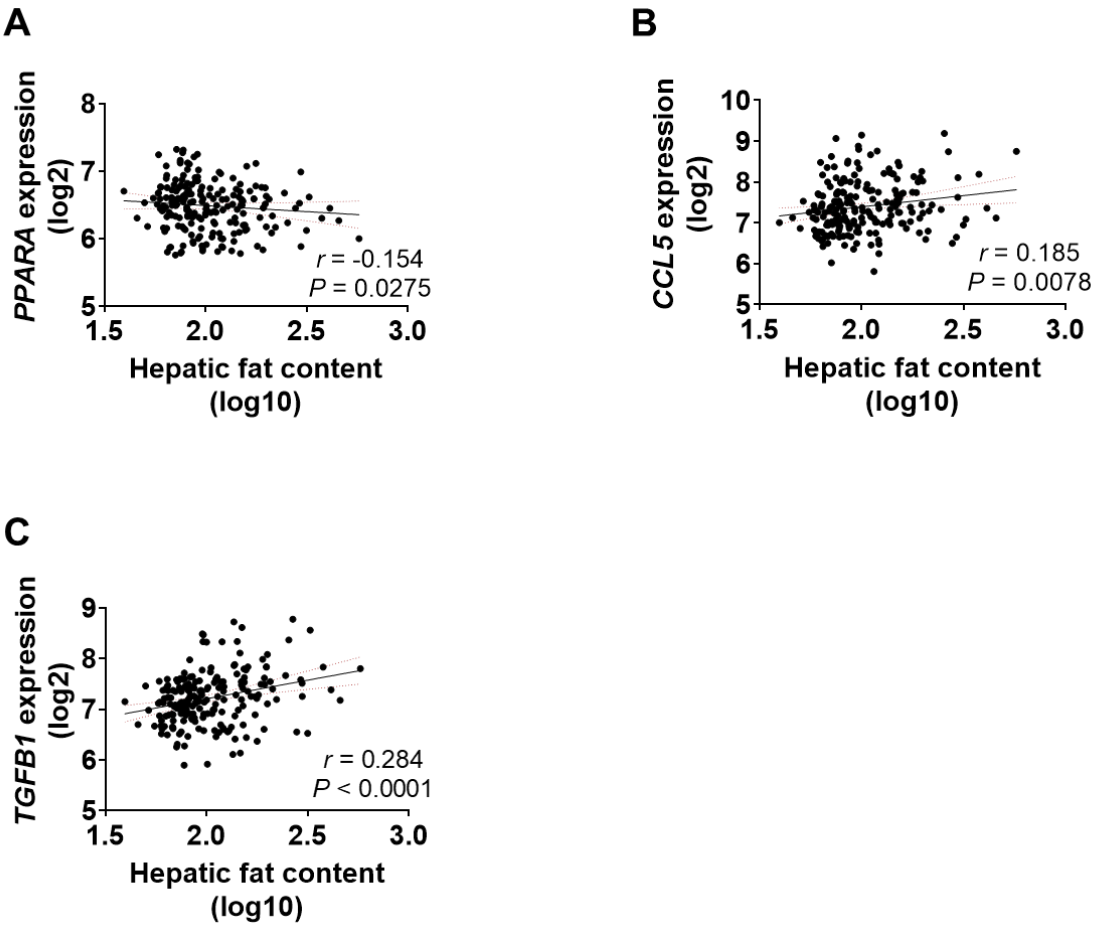

Fig. S2. Correlation between gene expression and hepatic fat in humans. Spearman's correlation between expression of **(A)** *PPARA*, **(B)** *CCL5*, **(C)** *TGFB1* and hepatic fat in livers from transplantation donors (n=206).

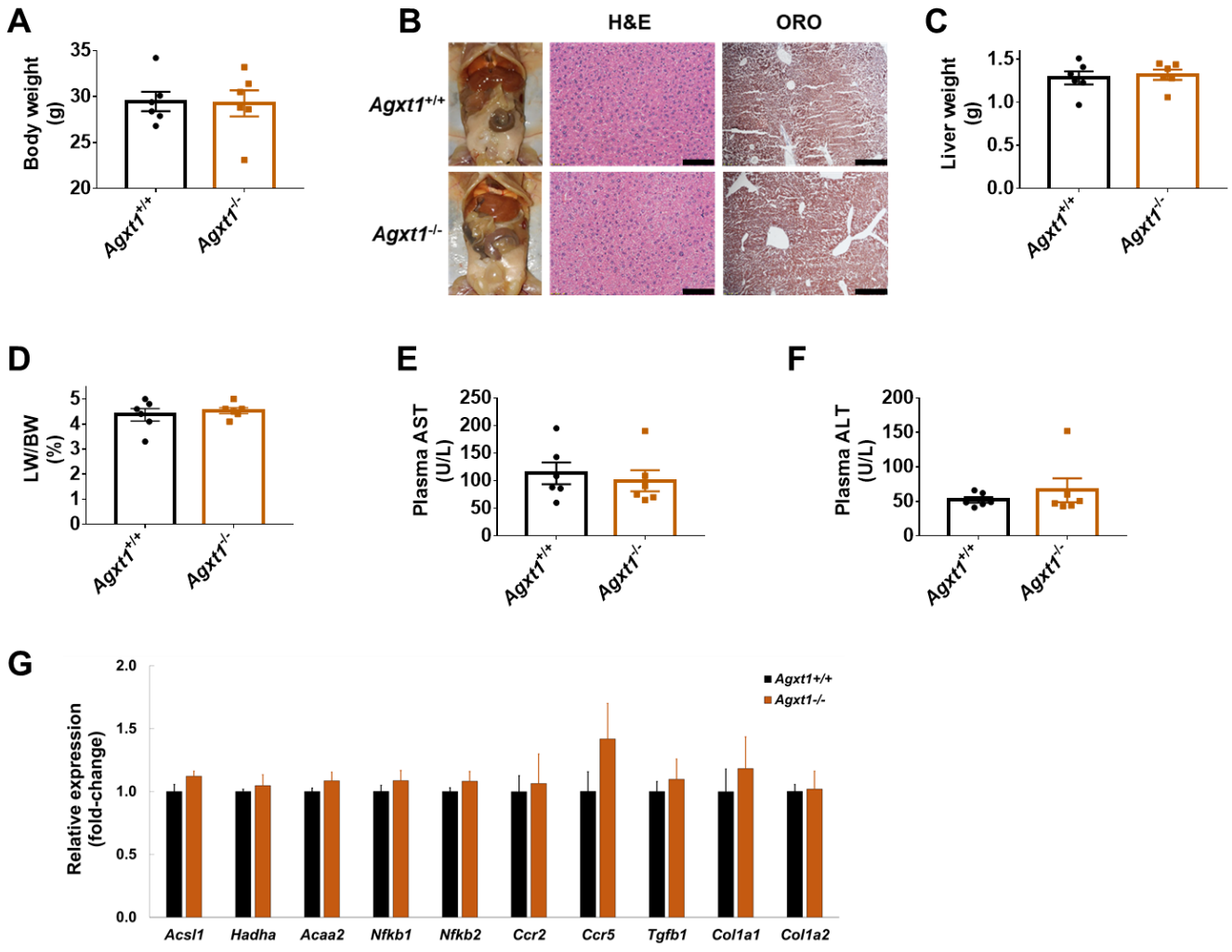

Fig. S3. *Agxt1*$^{+/+}$ and *Agxt1*$^{-/-}$ mice are comparable on CD. *Agxt1*$^{+/+}$ and *Agxt1*$^{-/-}$ mice were fed standard CD for 12 weeks (n=6): **(A)** Body weight, **(B)** gross appearance of the peritoneal cavities and histology using H&E and ORO staining (Scale bar: 50 μm for H&E, 100 μm for ORO), **(C)** liver weight, **(D)** ratio of liver weight to body weight (LW/BW %), **(E)** plasma AST, and **(F)** plasma ALT. **(G)** qPCR analysis of genes regulating FAO, inflammation and fibrosis in the liver. Data are means ± SEM. Statistical differences were compared using student's t test or Mann-Whitney U test.

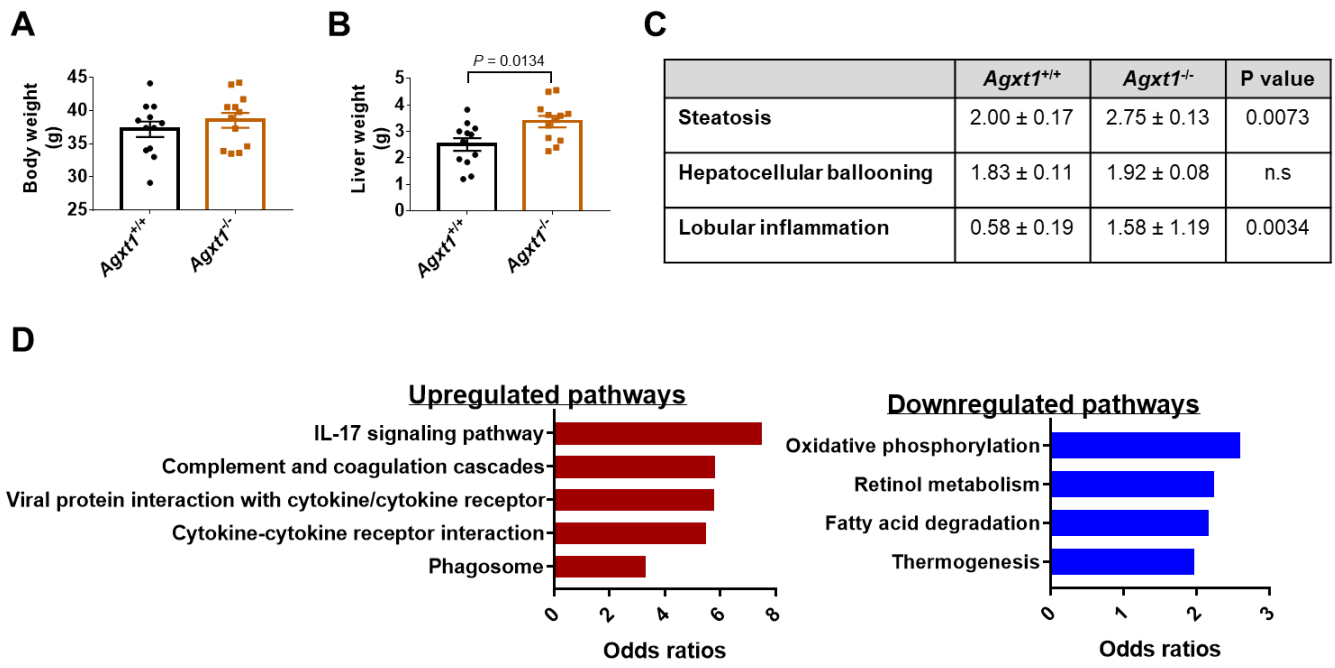

	Agxt1$^{+/+}$	*Agxt1*$^{-/-}$	P value
Steatosis	2.00 ± 0.17	2.75 ± 0.13	0.0073
Hepatocellular ballooning	1.83 ± 0.11	1.92 ± 0.08	n.s
Lobular inflammation	0.58 ± 0.19	1.58 ± 1.19	0.0034

Fig. S4. NAFLD-related parameters in *Agxt1*$^{+/+}$ and *Agxt1*$^{-/-}$ mice fed NASH-diet. *Agxt1*$^{+/+}$ and *Agxt1*$^{-/-}$ mice were fed NASH-diet for 12 weeks (n=12): **(A)** Body weight, **(B)** liver weight and **(C)** H&E-based scoring of steatosis, hepatocellular ballooning and lobular inflammation. Data are means ± SEM. Statistical differences were compared using Student's t test or Mann-Whitney U test. **(D)** Pathway analysis following RNA-sequencing of livers from *Agxt1*$^{+/+}$ and *Agxt1*$^{-/-}$ mice (n=4). Pathways enriched in the up- or down-regulated DEG are plotted in red or blue, respectively.

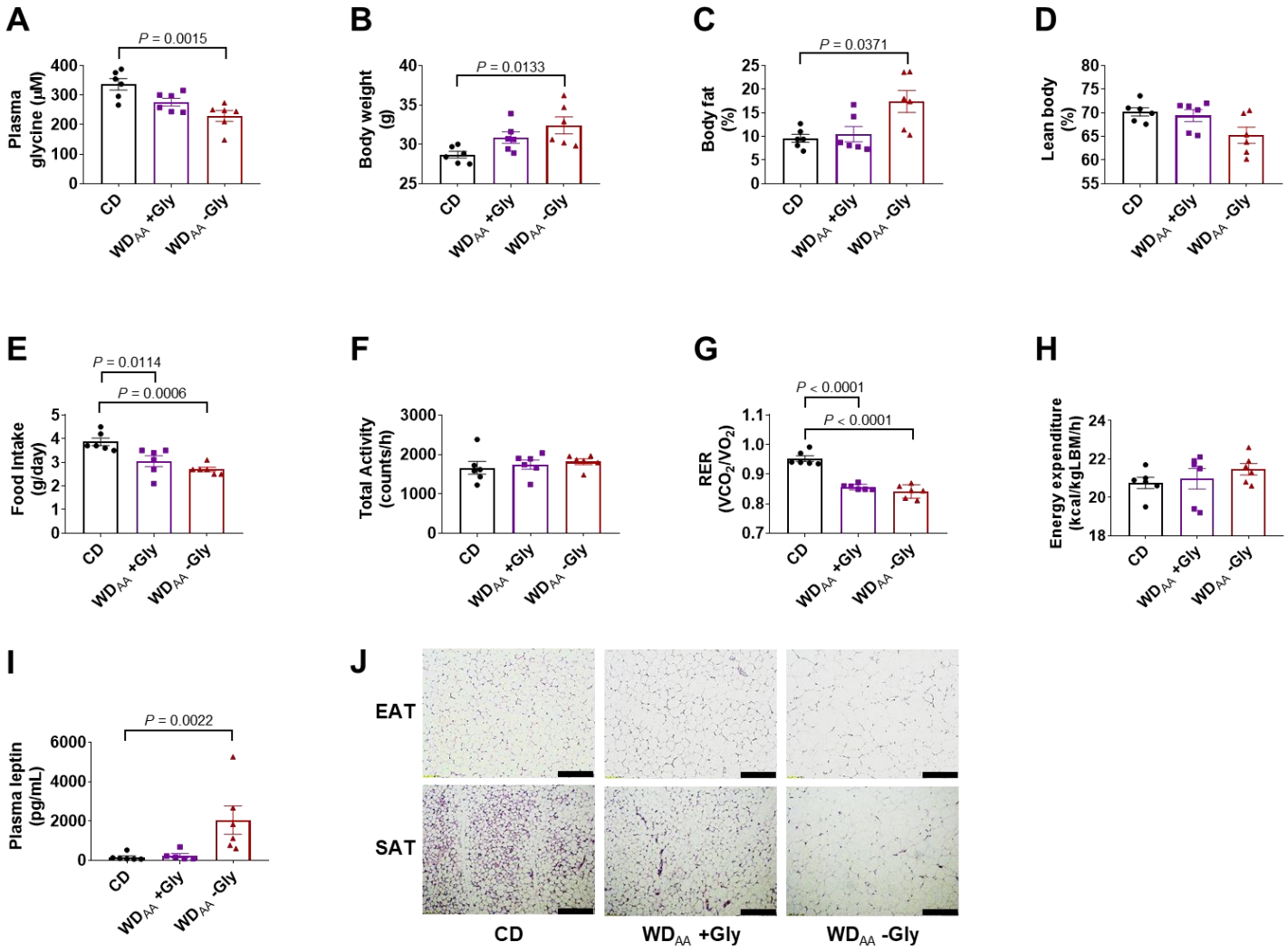

Fig. S5. Glycine deficiency exacerbates WD-induced obesity. *Apoe*$^{-/-}$ mice were fed CD, WD_{AA}+Gly or WD_{AA}-Gly for 10 weeks (n=6): **(A)** Plasma glycine. NMR-based body composition analysis: **(B)** Body weight, **(C)** fat (%), and **(D)** lean mass (%). CLAMS analysis: **(E)** Food intake, **(F)** total activity, **(G)** respiratory exchange ratio (RER), and **(H)** energy expenditure. **(I)** Plasma Leptin, and **(J)** H&E histology of epididymal and subcutaneous adipose tissues (EAT and SAT, Scale bar: 100 μm). Data are means ± SEM. Statistical differences were compared by one-way ANOVA followed by Bonferroni post-hoc test or by Kruskal-Wallis test followed by Dunn's post hoc-test.

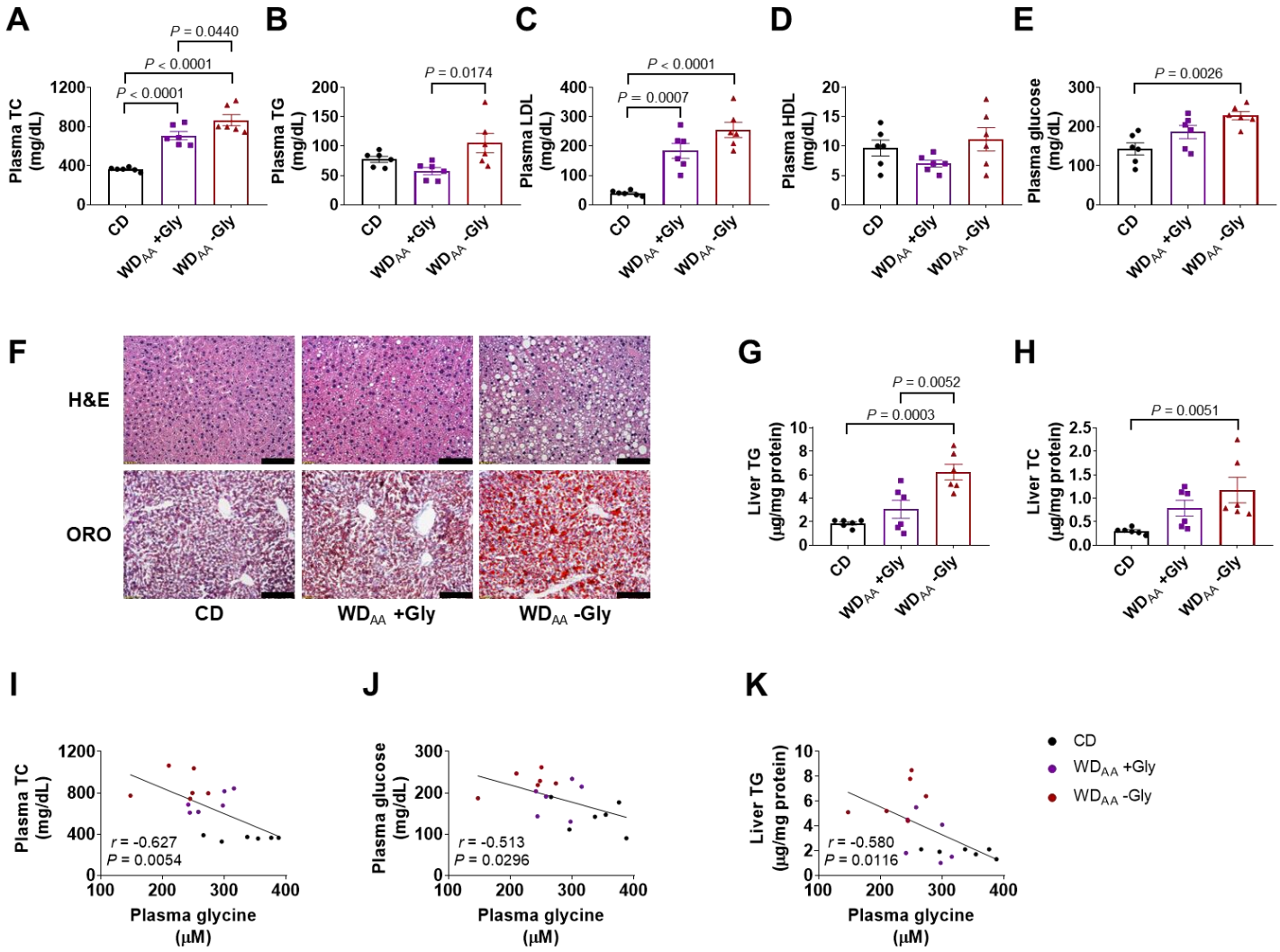

Fig. S6. Glycine deficiency exacerbates WD-induced hyperlipidemia and HS. *Apoe*$^{-/-}$ mice were fed CD, WD_{AA}+Gly or WD_{AA}-Gly for 10 weeks (n=6): **(A)** Plasma TC, **(B)** plasma TG, **(C)** plasma LDL, **(D)** plasma HDL, **(E)** plasma glucose, **(F)** liver histology using H&E and ORO staining (Scale bar: 50 µm for H&E, 100 µm for ORO), **(G)** liver TG and **(H)** liver TC. Data are means ± SEM. Statistical differences were compared by one-way ANOVA followed by Bonferroni post-hoc test or by Kruskal-Wallis test followed by Dunn's post-hoc test. Spearman's correlation analyses between plasma glycine and **(I)** Plasma TC, **(J)** plasma glucose and **(K)** liver TG.

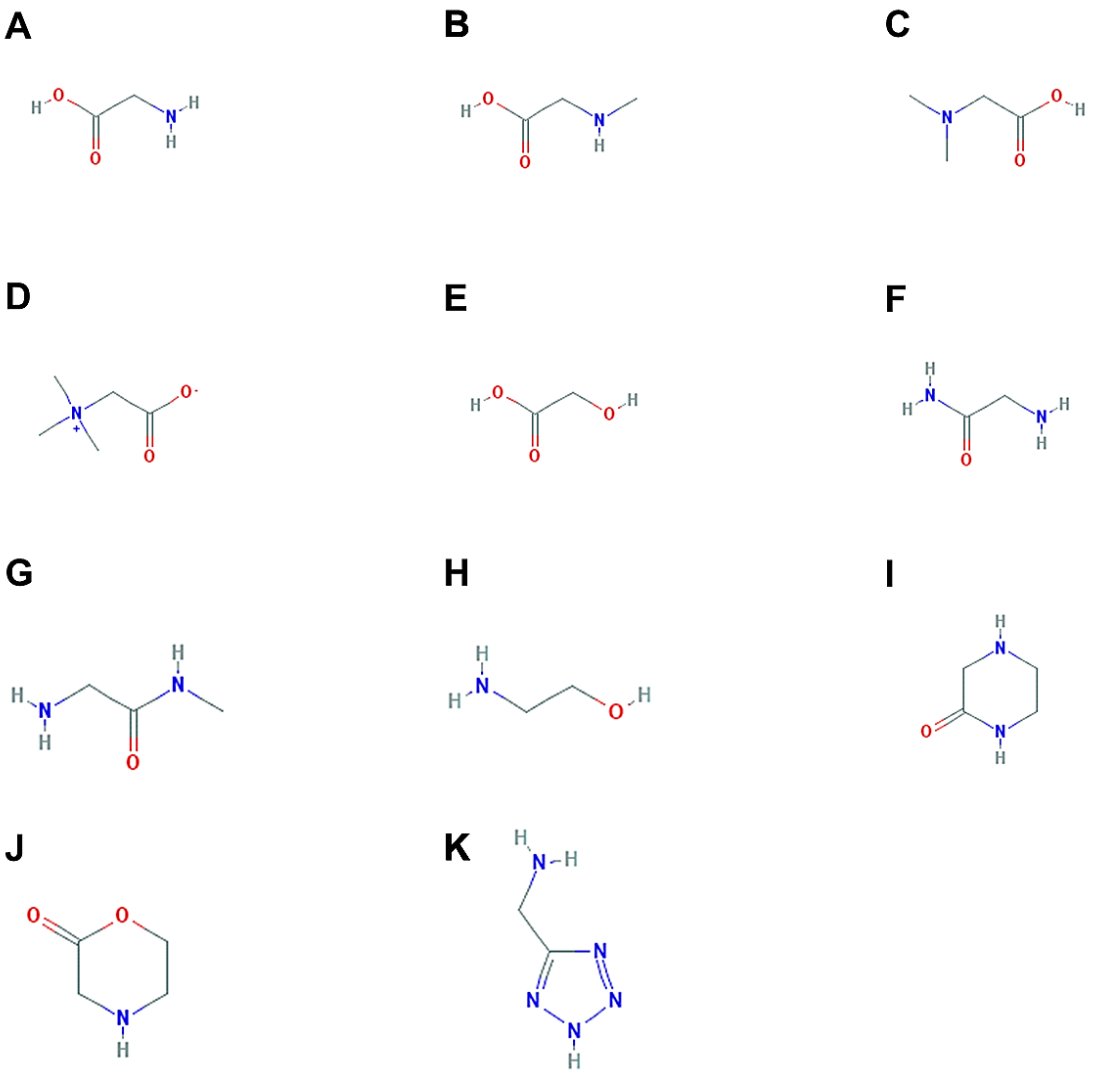

Fig. S7. Glycine-based compounds. Compounds structurally similar to glycine were chosen to evaluate structural, conformational, electrostatic or isosteric modifications to the glycine scaffold. **(A)** Glycine, **(B)** N-methylglycine, **(C)** N,N-dimethylglycine, **(D)** N,N,N-trimethylglycine, **(E)** Glycolic acid, **(F)** Glycinamide, **(G)** 2-amino-N-methylacetamide, **(H)** Ethanolamine, **(I)** 2-oxopiperazine, **(J)** Morpholin-2-one, and **(K)** (1H-tetrazol-5-yl) methanamine.

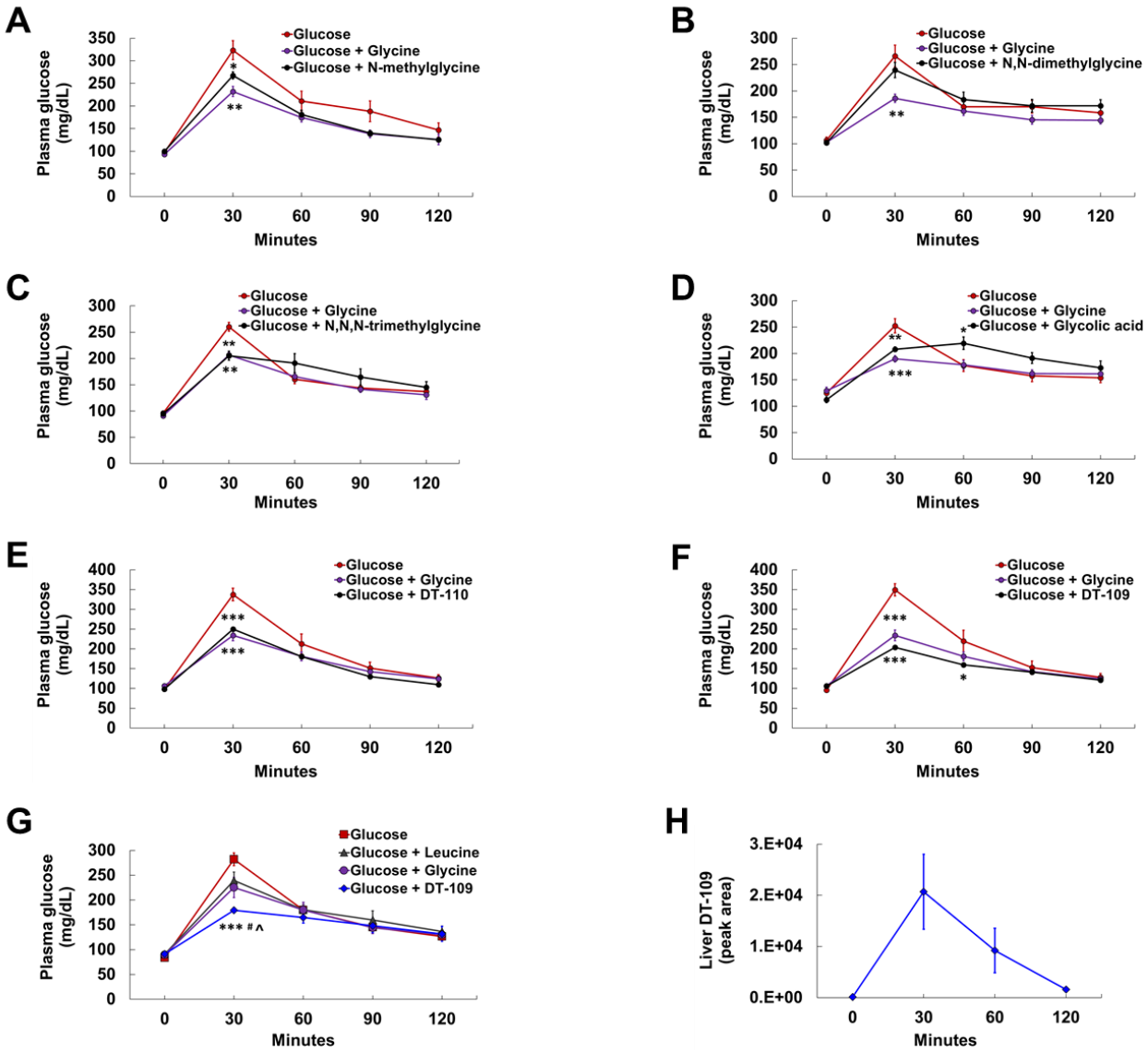

Fig. S8. Effects of glycine-based compounds on glucose tolerance. OGTT were performed in C57BL/6J mice after 12 h fasting (n=5-8). Mice received orally glucose alone (2 mg/g body weight), glucose with 0.5 mg/g body weight of glycine or with 0.5 mg/g body weight of glycine-based compounds: **(A)** N-methylglycine, **(B)** N,N-dimethylglycine, **(C)** N,N,N-trimethylglycine, **(D)** Glycolic acid, **(E)** DT-110 and **(F)** DT-109. **(G)** Mice received orally glucose alone (2 mg/g body weight), glucose with DT-109 (0.5 mg/g body weight) or equivalent amounts of free leucine or glycine (0.17 or 0.33 mg/g body weight, respectively). **(H)** LC-MS analysis of liver DT-109 before and after oral administration of DT-109 (0.5 mg/g body weight, n=3). Data are means ± SEM. Statistical differences were compared by one-way ANOVA followed by Bonferroni post-hoc test or by Kruskal-Wallis test followed by Dunn's post hoc-test. **P*<0.05, ***P*<0.01, ****P*<0.001 vs. glucose; $^{\#}$*P*<0.05 vs. leucine. ^*P*<0.05 vs. glycine.

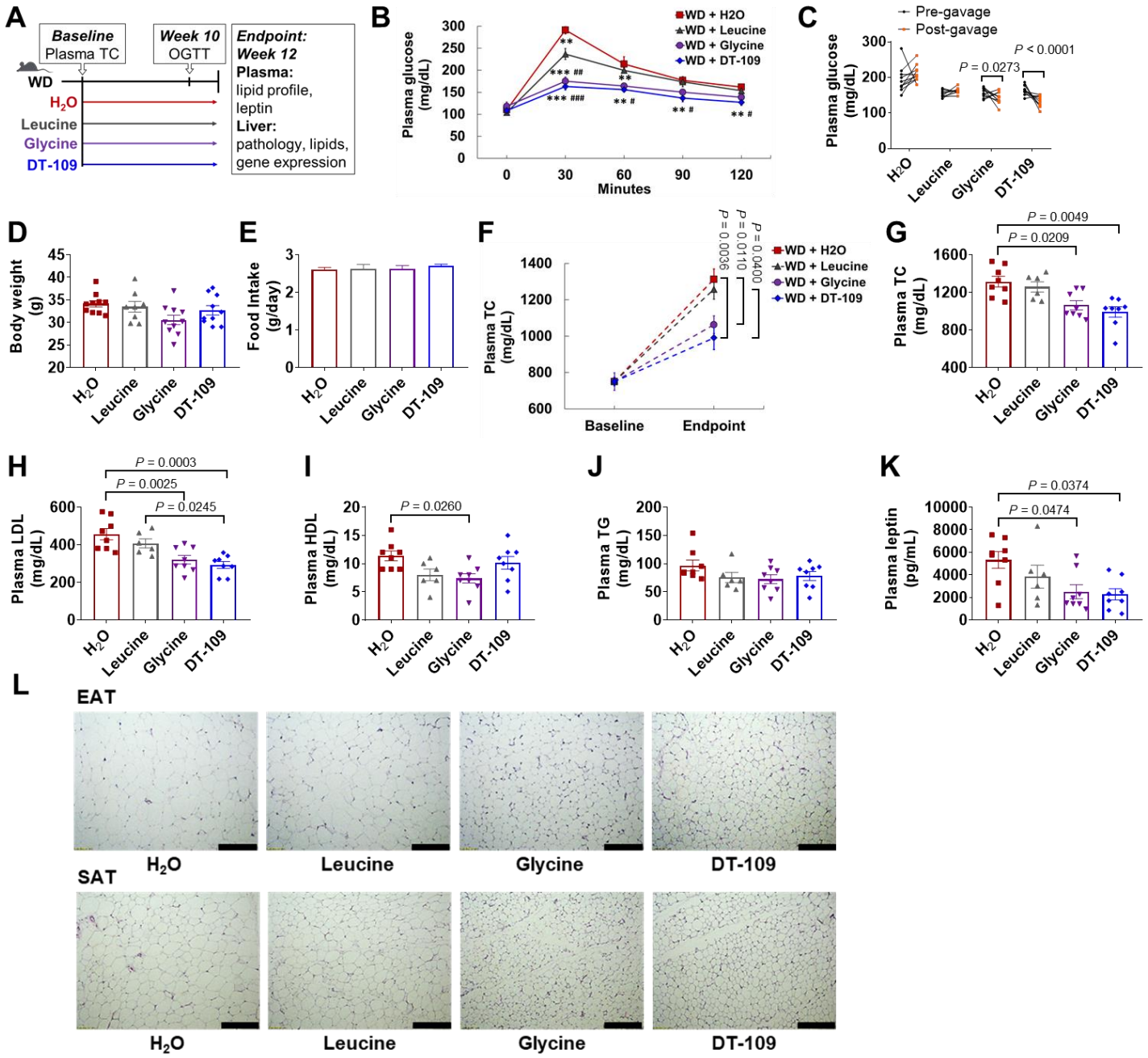

Fig. S9. Lipid-lowering effects of DT-109. (A) *Apoe*$^{-/-}$ mice were fed a standard WD and received orally DT-109 (1 mg/g body weight/day), equivalent amounts of free leucine or glycine (0.33 or 0.67 mg/g body weight/day) or H_2O for 12 weeks (n=8-10). **(B)** At week 10, OGTT was performed after 12 h fasting. Mice received orally glucose alone (2 mg/g body weight), glucose with 1 mg/g body weight of DT-109 or equivalent amounts of free leucine (0.33 mg/g body weight) or glycine (0.67 mg/g body weight). $^{**}P<0.01$, $^{***}P<0.001$ vs. H_2O; $^{\#}P<0.05$, $^{\#\#}P<0.01$, $^{\#\#\#}P<0.01$ vs. leucine. **(C)** Non-fasting blood glucose was measured before and after 30 min of daily gavage with DT-109, leucine, glycine or H_2O. **(D)** Endpoint body weight. **(E)** Average food intake. **(F)** Plasma TC at baseline (before randomization to experimental groups) and

endpoint. Endpoint plasma analyses (n=6-8): **(G)** TC, **(H)** LDL, **(I)** HDL, **(J)** TG and **(K)** Leptin. **(L)** H&E histology of epididymal and subcutaneous adipose tissues (EAT and SAT, Scale bar: 100 μm). Data are means ± SEM. Statistical differences were compared by one-way ANOVA followed by Bonferroni post-hoc test or by Kruskal-Wallis test followed by Dunn's post-hoc test.

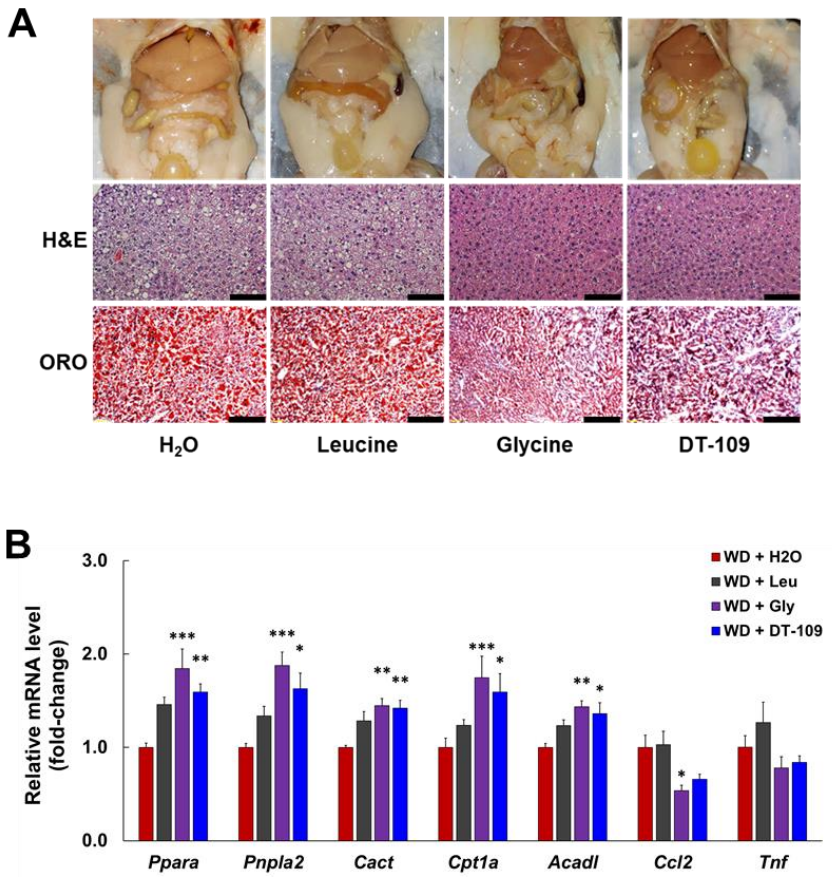

Fig. S10. Glycine or DT-109 prevent WD-induced HS. Endpoint liver analysis (n=7-10): **(A)** Gross appearance of the peritoneal cavities and histology using H&E and ORO (Scale bar: 50 μm for H&E, 100 μm for ORO). **(B)** qPCR analysis of key genes regulating FAO and inflammation relative to *Gapdh*. **P*<0.05, ***P*<0.01, ****P*<0.001 vs. WD+H_2O. Data are means ± SEM. Statistical differences were compared by one-way ANOVA followed by Bonferroni post-hoc test or by Kruskal-Wallis test followed by Dunn's post-hoc test.

A

	N (CD ; NASH)	CD	NASH	*P* value
Plasma glucose (mg/dL)	11 ; 50	108.5 ± 7.6	140.6 ± 4.6	0.0035
Plasma TC (mg/dL)	11 ; 50	148.3 ± 7.3	186.1 ± 6.1	0.0069
Plasma AST (U/L)	9 ; 30	62.3 ± 7.1	241.5 ± 28.4	< 0.0001
Plasma ALT (U/L)	9 ; 30	46.8 ± 4.7	195.7 ± 22.1	< 0.0001

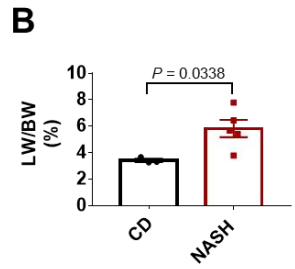

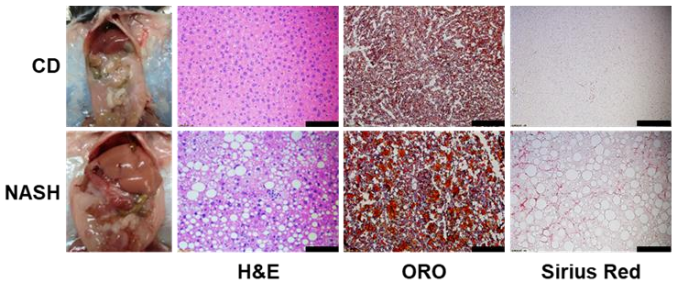

D

	N (CD ; NASH)	CD	NASH
Steatosis	3 ; 5	0.0 ± 0.0	2.2 ± 0.4
Hepatocellular ballooning	3 ; 5	0.0 ± 0.0	1.8 ± 0.2
Lobular inflammation	3 ; 5	0.0 ± 0.0	0.6 ± 0.2

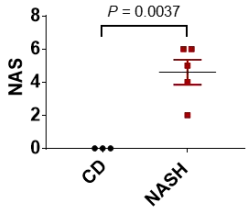

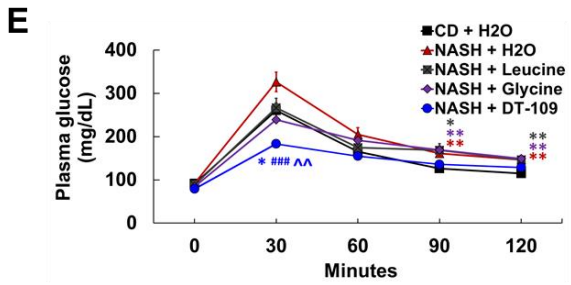

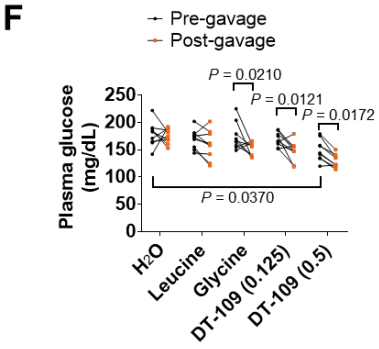

Fig. S11. Confirmation of NASH before randomization to experimental groups. C57BL/6J mice were fed CD (n=11) or NASH diet (n=50) for 12 weeks. **(A)** Fasting blood was collected from the submandibular vein for analysis of plasma glucose, TC, AST and ALT. A subset of the mice (CD: n=3, NASH-diet: n=5) was sacrificed to confirm liver pathology. **(B)** Liver weight to body weight ratio (LW/BW %). **(C)** Gross appearance of the peritoneal cavities and histology using H&E, ORO and Sirius Red staining (Scale bar: 50 μm for H&E and Sirius Red, 100 μm for ORO), **(D)** NAS as the sum of steatosis, hepatocellular ballooning and lobular inflammation scores. **(F)** At week 18, OGTT was performed after 12 h fasting (n=8-9). Mice received orally glucose alone (2 mg/g body weight), glucose with 0.5 mg/g body weight DT-109 or equivalent amounts of free leucine (0.17 mg/g body weight), glycine (0.33 mg/g body weight) or H_2O. **P*<0.05, ***P*<0.01 vs. CD+H_2O; $^{\#\#\#}$*P*<0.001 vs. NASH+H_2O; ^^*P*<0.01 vs. NASH+Leucine. **(G)** Non-fasting blood glucose before and after 30 min of daily gavage with DT-109, leucine, glycine or H_2O. Data are means ± SEM. Student's t test or Mann-Whitney U test were used to compare two groups. One-way ANOVA followed by Bonferroni post-hoc test or Kruskal-Wallis test followed by Dunn's post-hoc test were used to compare >2 groups.

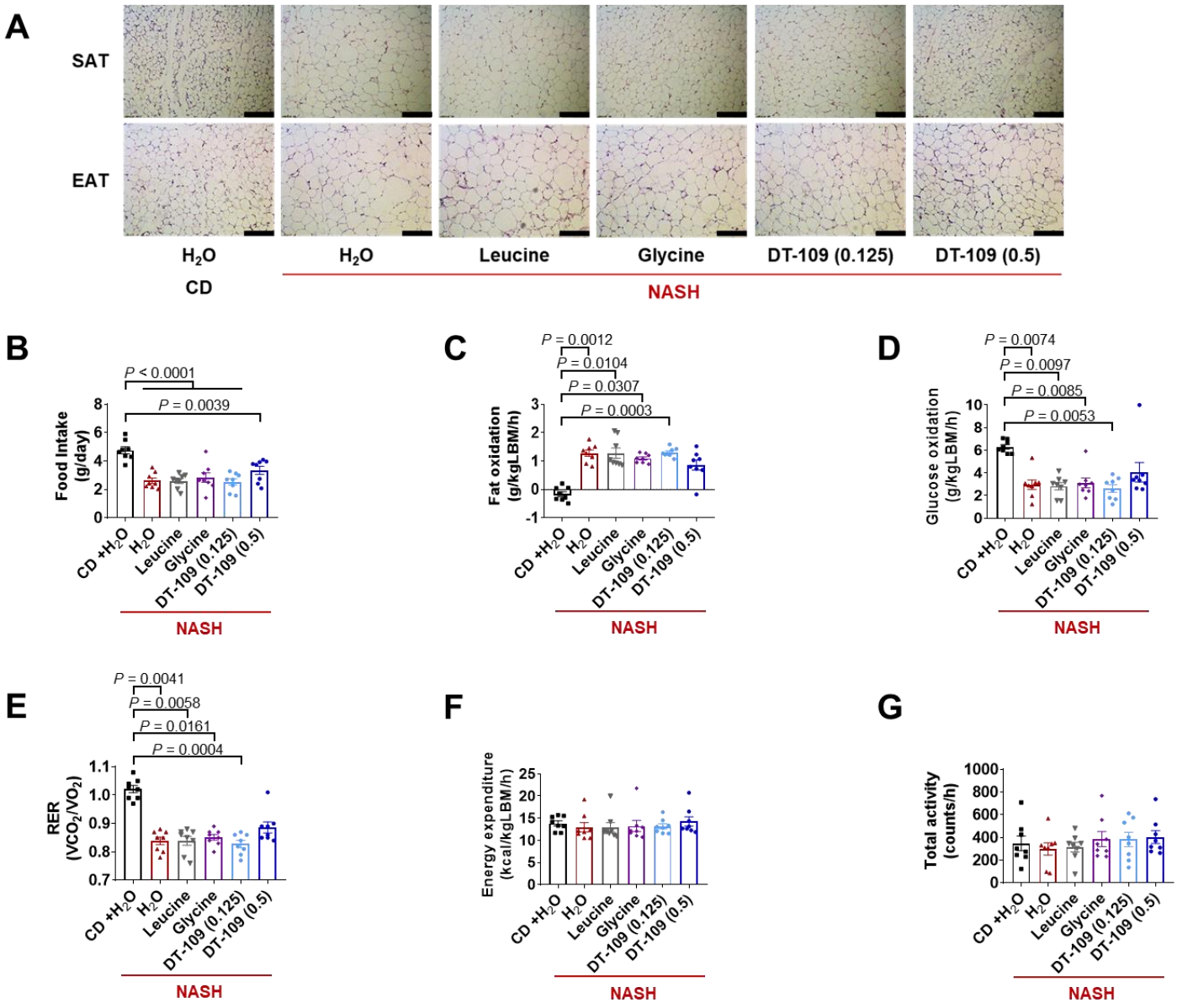

Fig. S12. Metabolic effects of DT-109 in mice with established NASH. C57BL/6J mice were fed CD or NASH-diet for 12 weeks. After NASH confirmation, mice were randomized to receive 0.125 or 0.5 mg/g body weight/day DT-109 or equivalent amounts of leucine or glycine (0.17 or 0.33 mg/g body weight/day) or H_2O via oral gavage for additional 12 weeks on NASH-diet. Mice fed CD and administered H_2O served as control (n=8-9). **(A)** H&E histology of epididymal and subcutaneous adipose tissues (EAT and SAT, Scale bar: 100 μm). CLAMS analysis at weeks 22-23: **(B)** Food intake, **(C)** fat oxidation, **(D)** glucose oxidation, **(E)** respiratory exchange ratio (RER), **(F)** energy expenditure and **(G)** total activity. LBM, lean body mass. Data are means ± SEM. Statistical differences were compared by one-way ANOVA followed by Bonferroni post-hoc test or by Kruskal-Wallis test followed by Dunn's post-hoc test.

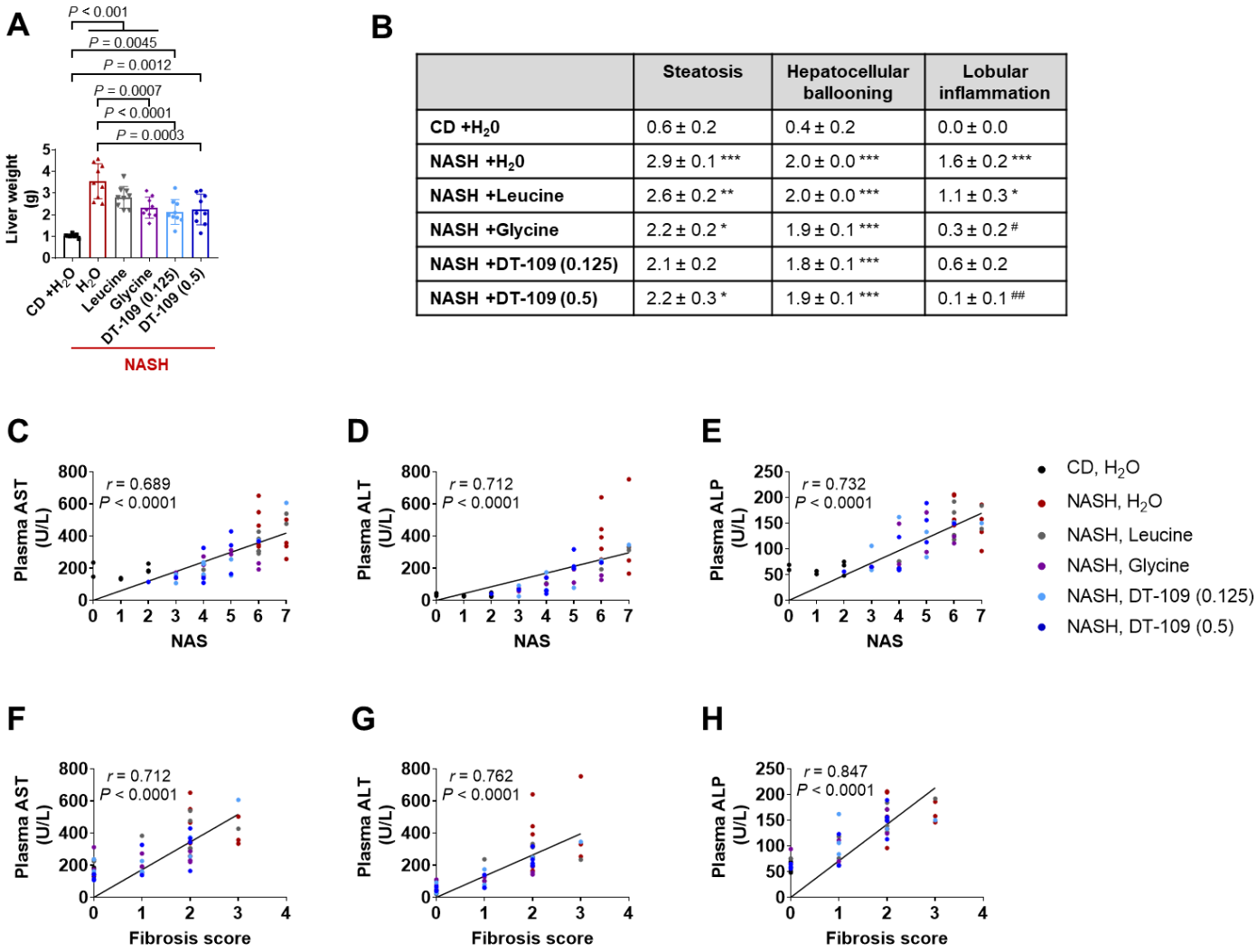

B

	Steatosis	Hepatocellular ballooning	Lobular inflammation
CD +$H_2$0	0.6 ± 0.2	0.4 ± 0.2	0.0 ± 0.0
NASH +$H_2$0	2.9 ± 0.1 ***	2.0 ± 0.0 ***	1.6 ± 0.2 ***
NASH +Leucine	2.6 ± 0.2 **	2.0 ± 0.0 ***	1.1 ± 0.3 *
NASH +Glycine	2.2 ± 0.2 *	1.9 ± 0.1 ***	0.3 ± 0.2 #
NASH +DT-109 (0.125)	2.1 ± 0.2	1.8 ± 0.1 ***	0.6 ± 0.2
NASH +DT-109 (0.5)	2.2 ± 0.3 *	1.9 ± 0.1 ***	0.1 ± 0.1 ##

Fig. S13. DT-109 protects against diet-induced NASH. C57BL/6J mice were fed CD or NASH-diet for 12 weeks. After NASH confirmation, mice were randomized to receive 0.125 or 0.5 mg/g body weight/day DT-109 or equivalent amounts of leucine or glycine (0.17 or 0.33 mg/g body weight/day) or H_2O via oral gavage for the additional 12 weeks on NASH-diet. Mice fed CD and administered H_2O served as control (n=8-9). **(A)** Liver weight, and **(B)** H&E-based scoring of steatosis, hepatocellular ballooning and lobular inflammation. *P<0.05, **P<0.01, ***P<0.001 vs. CD+H_2O; $^{\#}$P<0.05, $^{\#\#}$P<0.01 vs. NASH+H_2O. Data are means ± SEM. Statistical differences were compared by one-way ANOVA followed by Bonferroni post-hoc test or by Kruskal-Wallis test followed by Dunn's post-hoc test. Spearman's correlation analyses between NAS and plasma **(C)** AST, **(D)** ALT and **(E)** ALP. Spearman's correlation analyses between hepatic fibrosis score and plasma **(F)** AST, **(G)** ALT and **(H)** ALP.

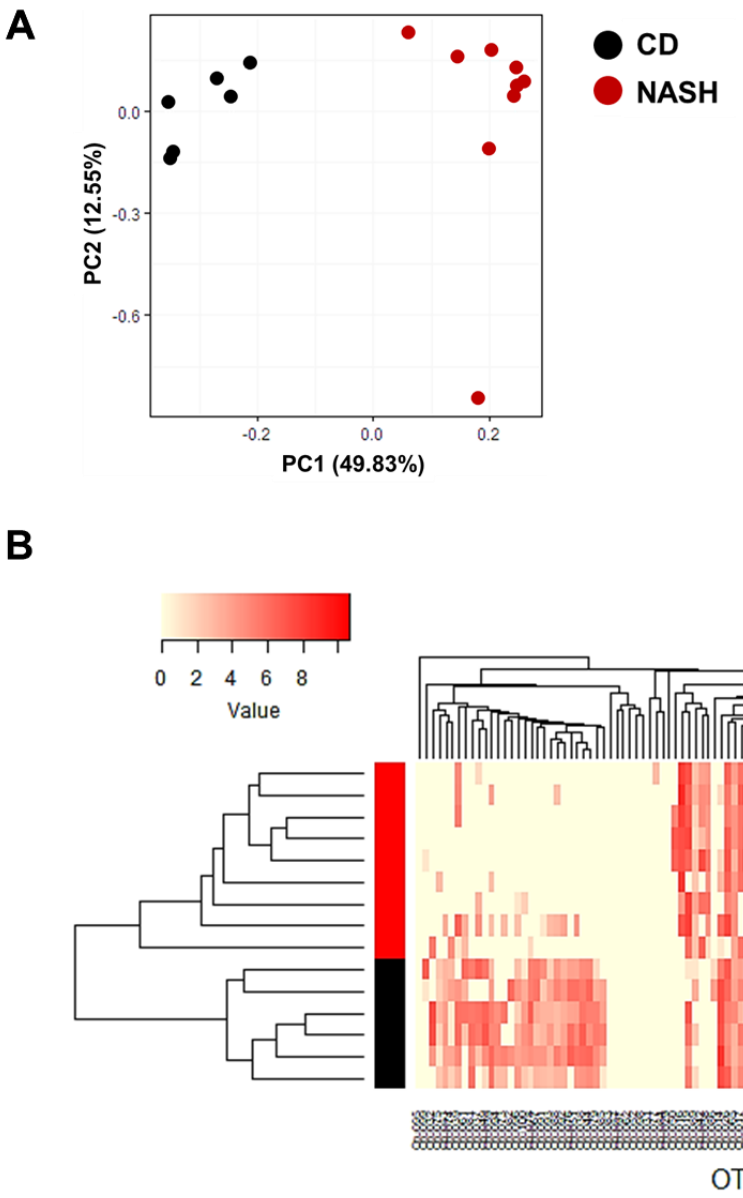

Fig. S14. Major shifts in the gut microbiome of mice with NASH. Fecal samples were obtained from mice fed CD or NASH-diet for 12 weeks before randomization to experimental groups (n=6-9 cages). Bacterial population was assessed using 16S rDNA sequencing. **(A)** PCA and **(B)** OTUs of fecal microbiomes in the CD and the NASH-diet groups.

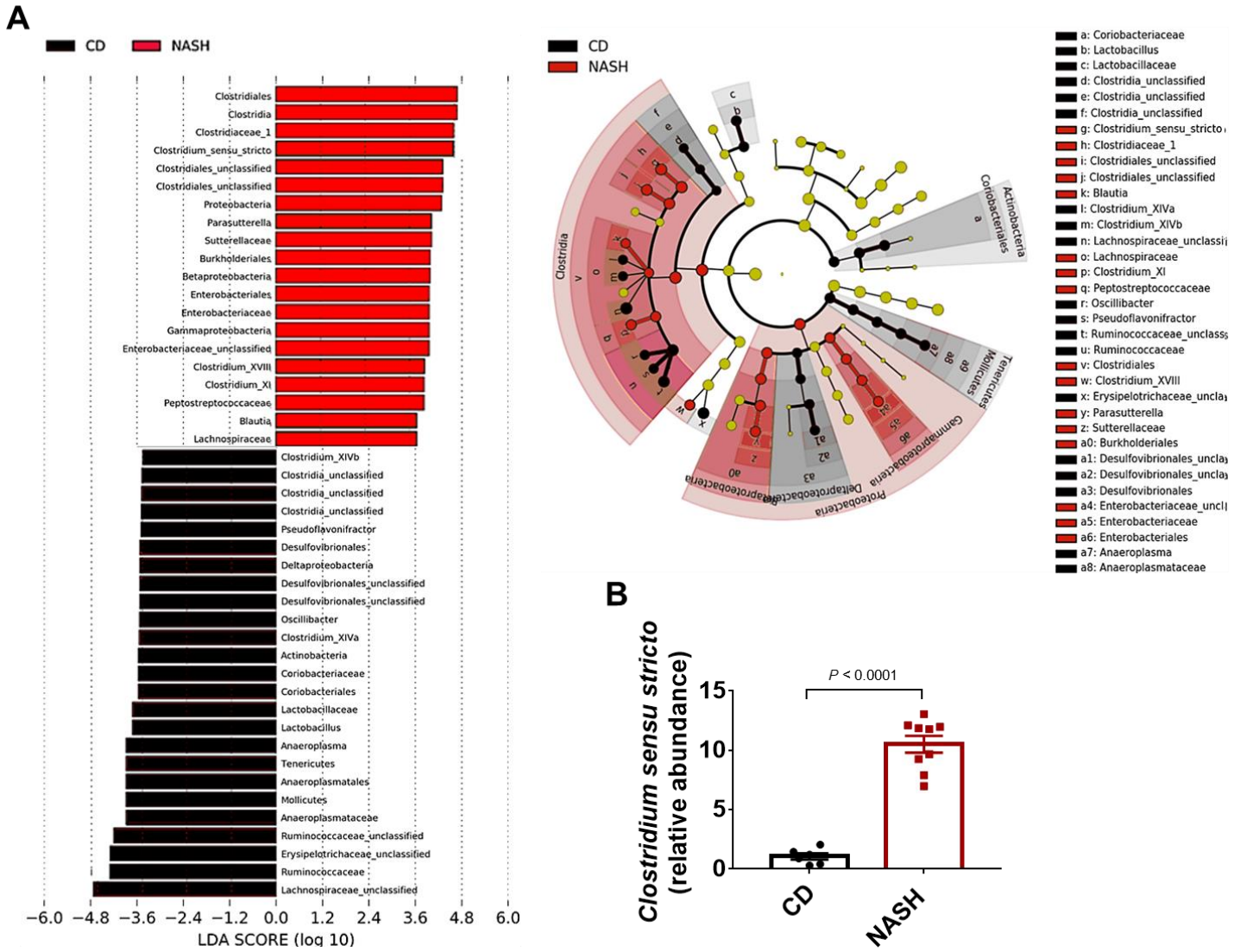

Fig. S15. *Clostridium sensu stricto* is overrepresented in mice with NASH. Fecal samples were obtained from mice fed CD or NASH-diet for 12 weeks. Bacterial population was assessed using 16S rDNA sequencing (n=6-9 cages). **(A)** Linear discriminant analysis (LDA) of overrepresented bacterial taxa in the CD group (black) and the NASH-diet group (red) identified by LEfSe. **(B)** 16S rDNA gene sequencing analysis of the *Clostridium sensu stricto* genus abundance in mice fed CD or NASH-diet for 12 weeks. Data are means ± SEM. Statistical differences were compared using Student's t test.

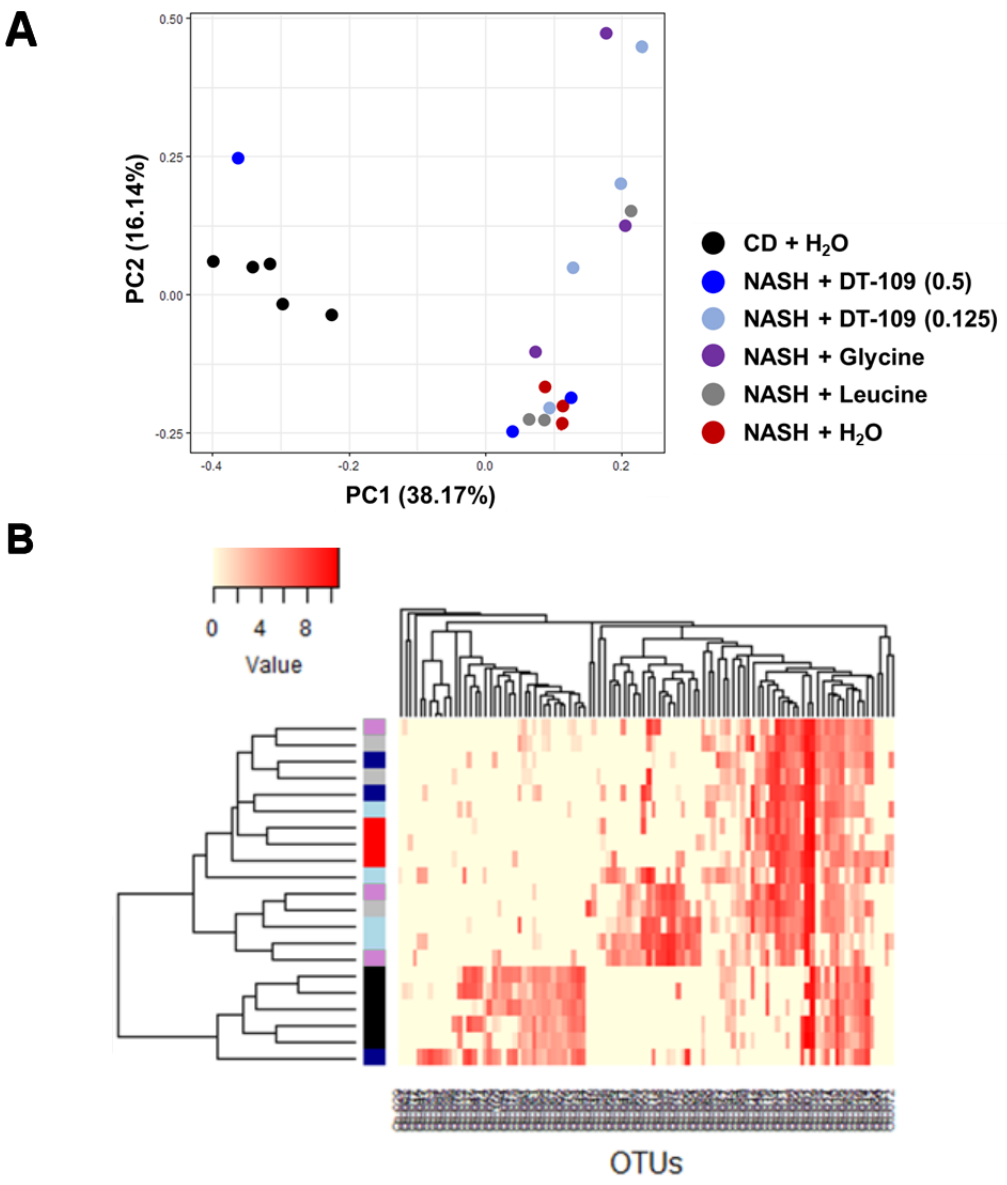

Fig. S16. Gut microbiome alterations after 2 weeks of treatments while on NASH-diet. Fecal samples were obtained from mice fed CD or NASH-diet for 12 weeks and then randomized to receive DT-109 at 0.125 or 0.5 mg/g body weight /day or equivalent amounts of free leucine (0.17 mg/g body weight /day), glycine (0.33 mg/g body weight /day) or H_2O via oral gavage for additional 2 weeks on NASH-diet feeding. Mice fed CD and administered H_2O served as control. Bacterial population was assessed using 16S rDNA sequencing (n=3-5 cages). **(A)** PCA and **(B)** hierarchical clustering of OTUs of fecal microbiomes in the different groups.

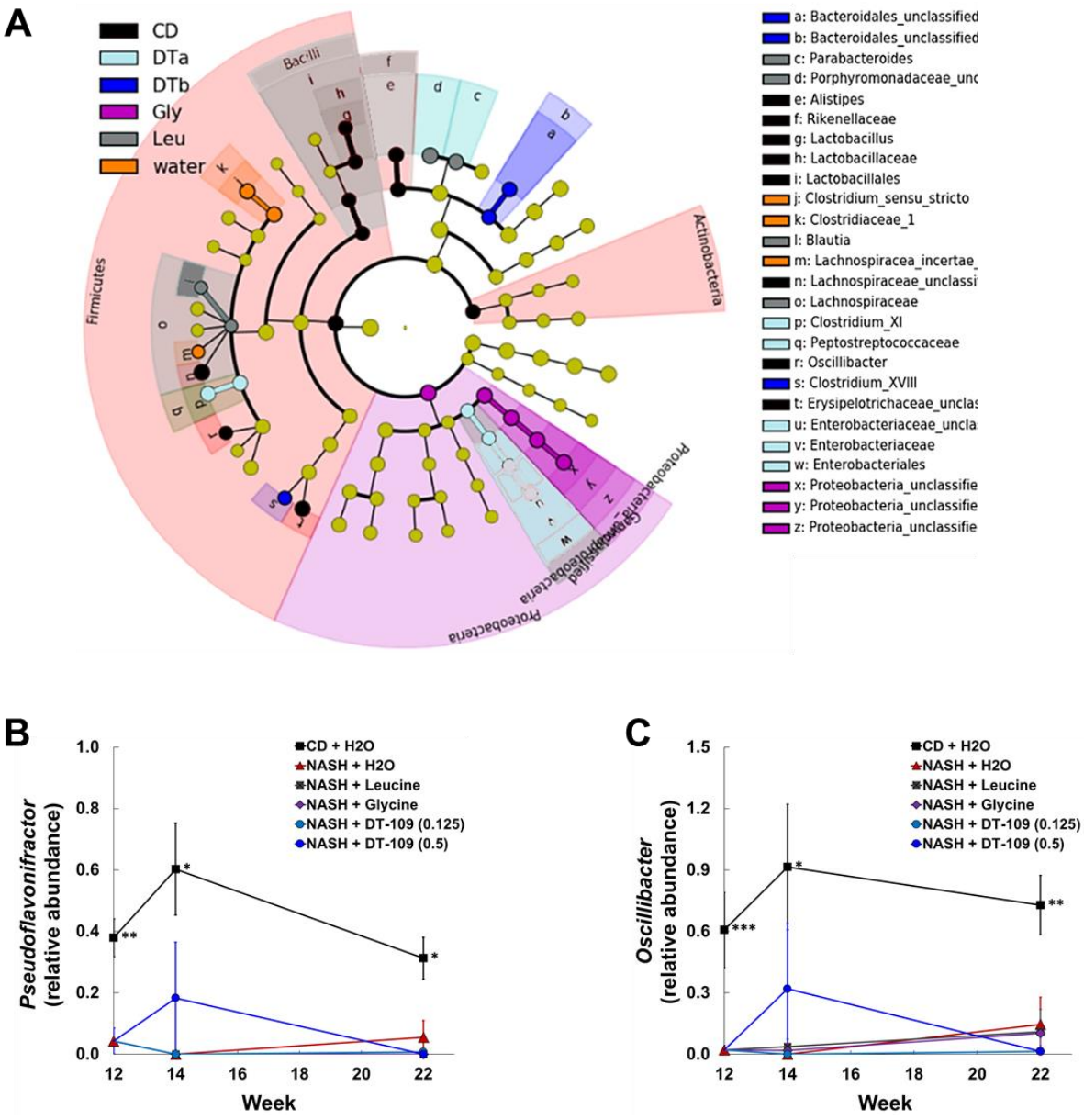

Fig. S17. Gut microbiome alterations after 10 weeks of treatments while on NASH-diet. Fecal samples were obtained from mice fed CD or NASH-diet for 12 weeks and then randomized to receive DT-109 at 0.125 (DTa) or 0.5 (DTb) mg/g body weight /day or equivalent amounts of free leucine (0.17 mg/g body weight /day), glycine (0.33 mg/g body weight /day) or H_2O via oral gavage for additional 10 weeks on NASH-diet feeding. Mice fed CD and administered H_2O served as control. Bacterial population was assessed using 16S rDNA sequencing (n=3-5 cages). **(A)** Overrepresented bacterial taxa in each group were identified by LEfSe. Relative abundance of the genera **(B)** *Pseudoflavonifractor* and **(C)** *Oscillibacter* in fecal samples from each group before (week 12) and after 2 or 10 weeks of treatments (weeks 14 or 22, respectively, as shown in Fig. 4A). **P*<0.05, ***P*<0.01, ****P*<0.001 vs. NASH before treatments. Data are means ±SEM. Statistical differences were compared by one-way ANOVA followed by Bonferroni post-hoc test or by Kruskal-Wallis test followed by Dunn's post-hoc test.

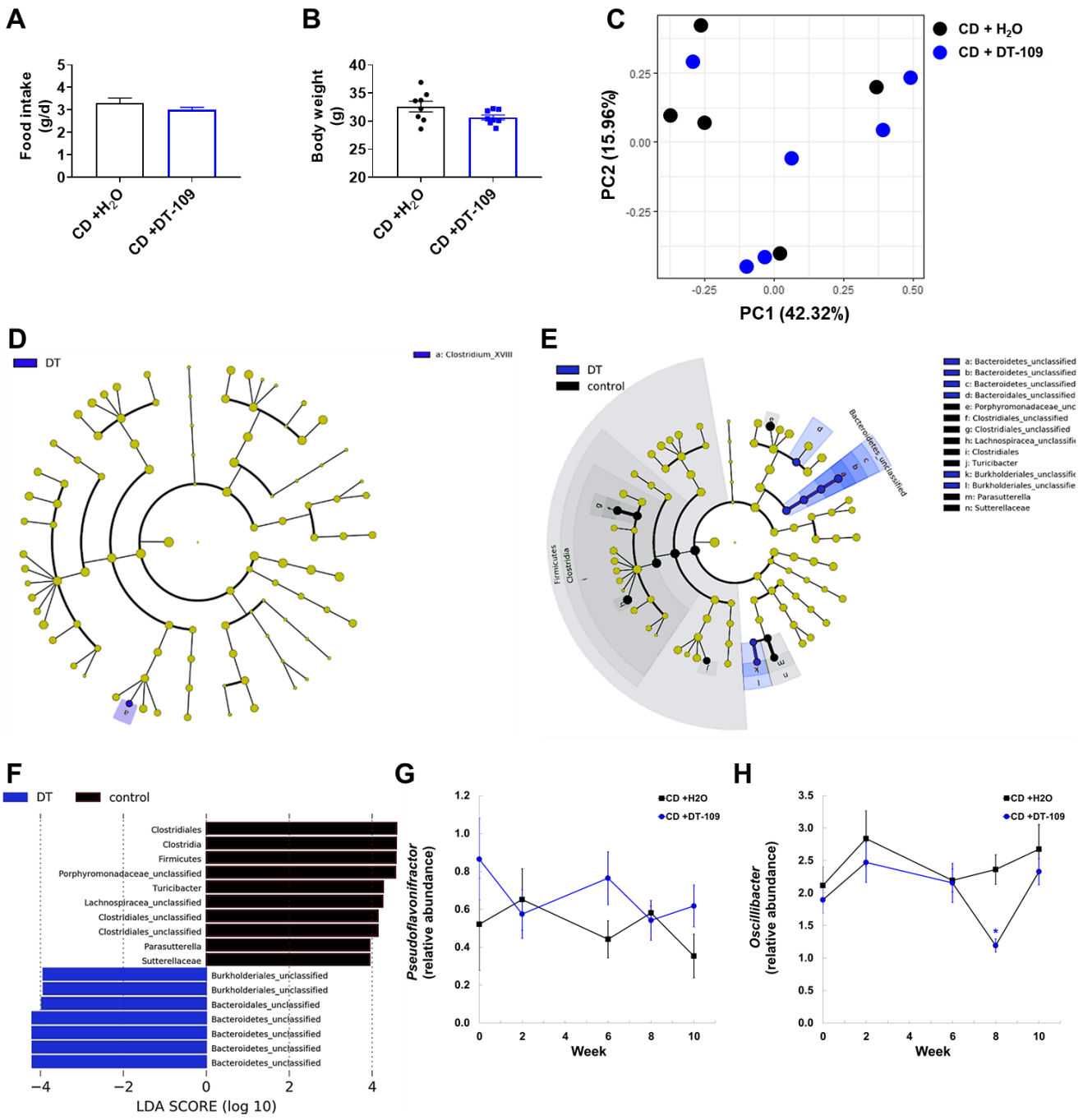

Fig. S18. Gut microbiome alterations during DT-109 treatment while on CD. C57BL/6J mice were fed CD and treated with 0.5 mg/g body weight/day of DT-109 for 10 weeks. **(A)** Food intake. **(B)** Endpoint body weight (n=8 mice). Fecal samples were obtained at baseline and after 2, 6, 8 and 10 weeks of DT-109 treatment. Bacterial population was assessed using 16S rDNA sequencing (n=5-7 cages). **(C)** PCA and **(D)** LEfSe at baseline. **(E)** LEfSe and **(F)** LDA at endpoint. Relative abundance of the genera **(G)** *Pseudoflavonifractor* and **(H)** *Oscillibacter* in fecal samples from each group throughout the study. Data are means ± SEM. Statistical differences were compared using Student's t test.

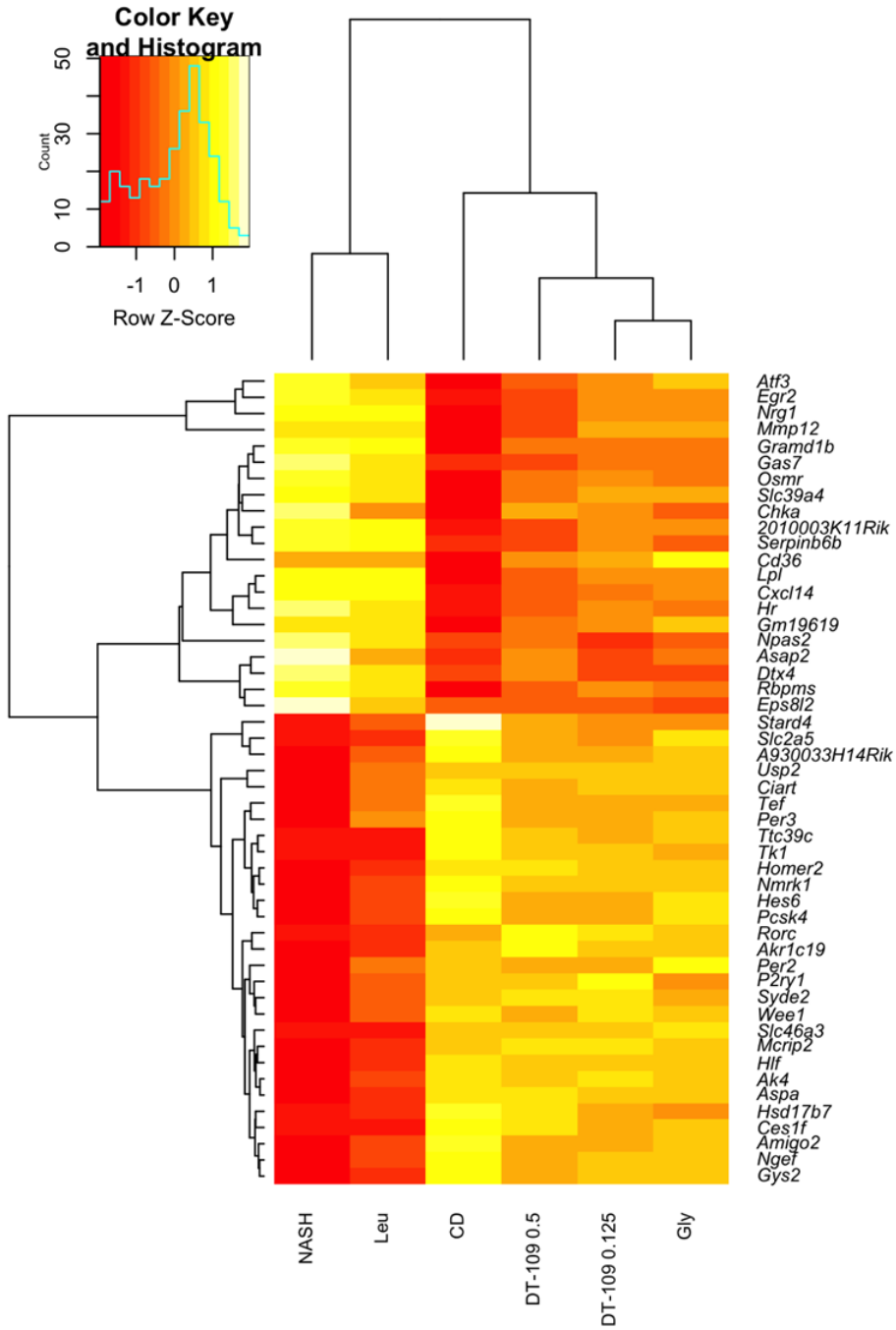

Fig. S19. DT-109 reverses NASH-diet-induced liver transcriptome alterations. Heatmap-based representation of the top 50 DEG across all experimental groups as determined by log2fold-chage compared with CD group. Each row represents one gene, and each column represents one comparison to CD group (n=4).

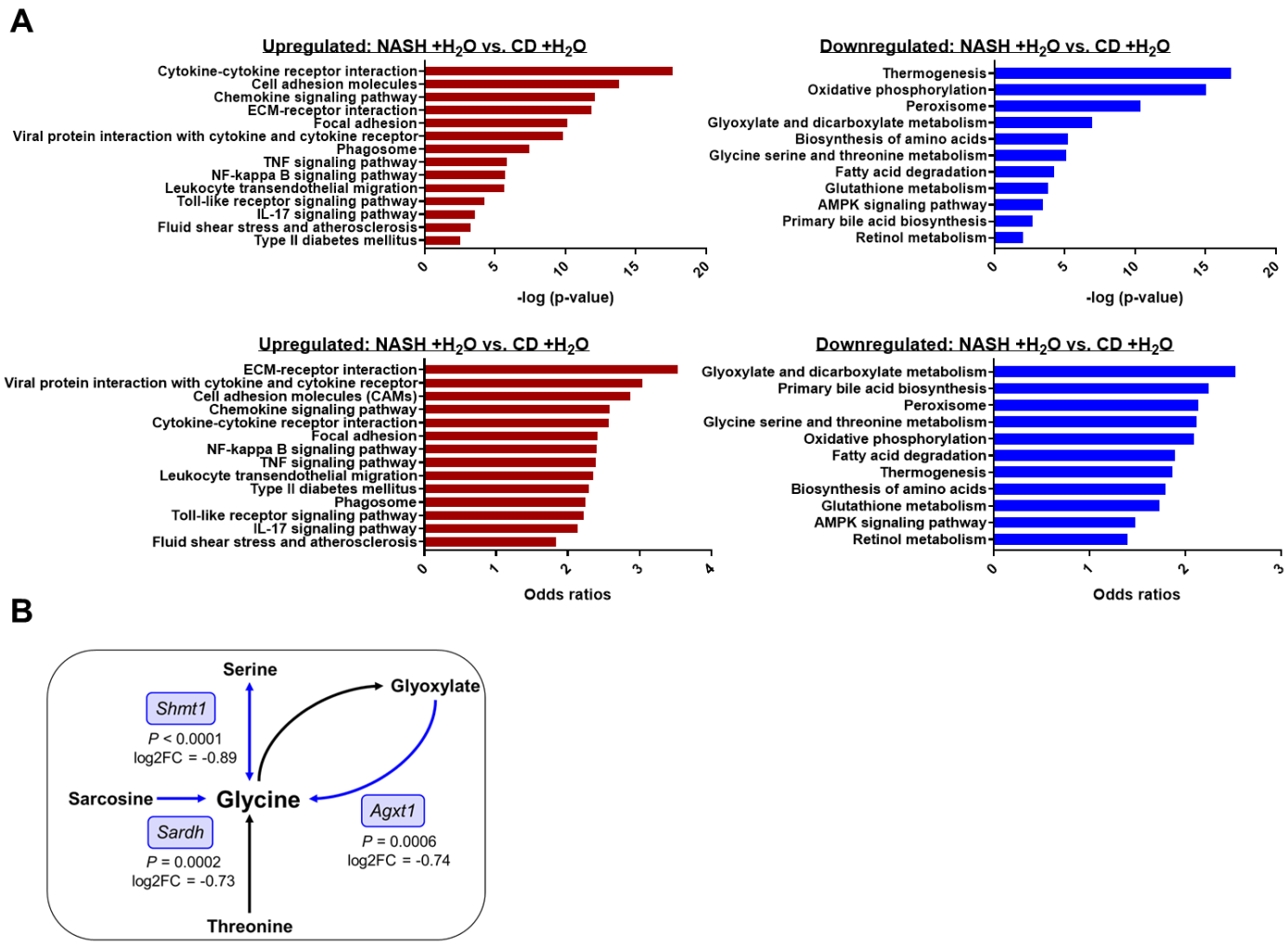

Fig. S20. Pathway analysis of livers from mice on CD vs. NASH-diet. **(A)** Pathways enriched in the upregulated DEG are plotted in red, while pathways enriched in the down-regulated DEG are plotted in blue. **(B)** Changes in glycine biosynthetic genes/pathways analyzed by RNA-sequencing of livers from mice on CD+H_2O vs. NASH+H_2O and pathway analysis (n=4). The significance of the enriched pathways was determined by right-tailed Fisher's exact test followed by Benjamini-Hochberg multiple testing adjustment.

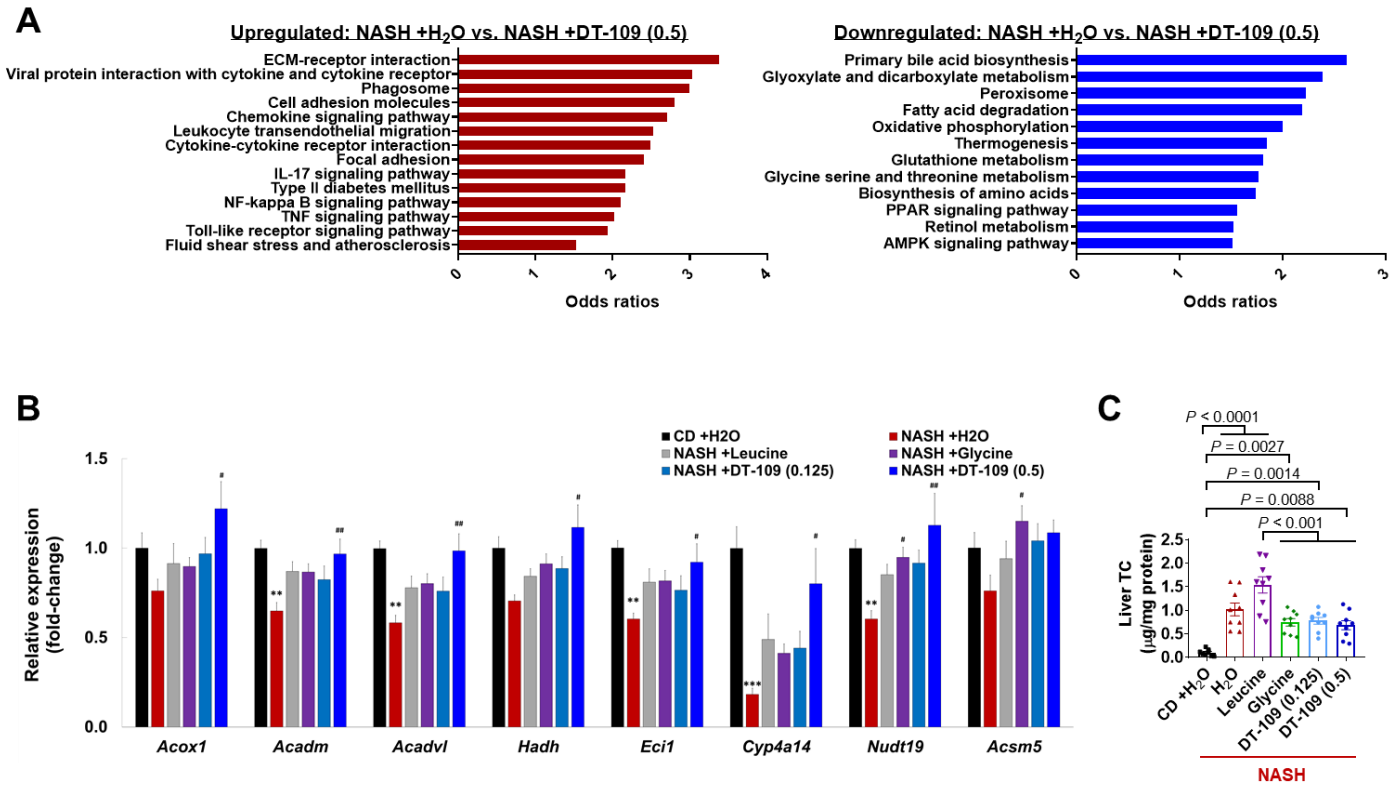

Fig. S21. Pathway analysis of livers from mice on NASH and treated with H_2O vs. DT-109. (A) Pathways enriched in the upregulated DEG are plotted in red, while pathways enriched in the down-regulated DEG are plotted in blue. **(B)** qPCR validation of FAO-related DEG (n=8). **P<0.01, ***P<0.001 vs. CD+H_2O; $^{\#}$P<0.05, $^{\#\#}$P<0.01 vs. NASH+H_2O. **(C)** Liver TC (n=8-9). Data are means ± SEM. Statistical differences were compared by one-way ANOVA followed by Bonferroni post-hoc test or by Kruskal-Wallis test followed by Dunn's post-hoc test.

Supplementary Tables

Table S1. Previous clinical evidences associating lower circulating glycine with NAFLD and other cardiometabolic diseases.

Cardiometabolic disease	N human subjects	Circulating glycine outcome
NAFLD (*7*)	Training dataset: 1535 Healthy vs. 465 NAFLD Validation dataset: 1661 Healthy vs. 499 NAFLD	Glycine was decreased while the majority of AA were increased in patients with NAFLD
NAFLD (*8*)	86 (varying degrees of hepatic steatosis)	Glycine was negatively correlated with hepatic steatosis
NAFLD (*9*)	20 Healthy vs. 44 NAFLD	Glycine was decreased in patients with NAFLD and negatively correlated with hepatocyte ballooning and lobular inflammation
Obesity (*11*)	67 Lean vs. 74 Obese	Glycine was decreased while various AA increased in obese patients
T2D (*12*)	Meta-analysis including 8,000 subjects (1940 with T2D)	Glycine was inversely associated with prediabetes and T2D
MetS (*13*)	472 (population study)	Glycine was negatively correlated with waist circumference, plasma TG, and MetS and positively correlated with HDL
Acute myocardial infarction (AMI) (*14*)	4109 (with suspected stable angina pectoris)	Glycine was inversely associated with the risk of AMI and positively associated with lower prevalence of obesity, T2D and a favorable lipid profile (higher HDL and apoA1, lower TG)
Coronary heart disease (CHD) (*15*)	11,147 (2053 with CHD)	Glycine was associated with lower risk of CHD and myocardial infarction

Table S2. Composition of the amino acid-defined WD with or without glycine (WD_{AA} +/-Gly). AA, amino acid.

Selected nutrient information	WD_{AA}+Gly	WD_{AA}-Gly
Protein (% of kcal)	22.4	22.5
Carbohydrates (% of kcal)	35.4	35.2
Fat (% of kcal)	42.2	42.3
Calorie density (kcal/g)	4.5	4.5
Sucrose (g/kg)	345.5	345.5
Maltodextrin (g/kg)	20.0	20.2
Anhydrous milk fat (g/kg)	210.0	210.0
Cholesterol (g/kg)	1.5	1.5
L-Alanine (g/kg)	14.4	14.4
L-Arginine (g/kg)	15.7	15.7
L-Asparagine (g/kg)	5.3	8.1
L-Aspartate (g/kg)	28.1	33.8
L-Cysteine (g/kg)	3.9	3.9
L-Glutamate (g/kg)	47.4	47.7
L-Glutamine (g/kg)	28.7	31.8
Glycine (g/kg)	**12.8**	**0**
L-Histidine (g/kg)	8.4	8.4
L-Isoleucine (g/kg)	10.6	10.6
L-Leucine (g/kg)	18.9	18.9
L-Lysine (g/kg)	18.5	18.5
L-Methionine (g/kg)	5.9	5.9
L-Phenylalanine (g/kg)	11.1	11.1
L-Proline (g/kg)	14.7	19.6
L-Serine (g/kg)	11.8	11.8
L-Threonine (g/kg)	9.7	9.7
L-Tryptophan (g/kg)	2.8	2.8
L-Tyrosine (g/kg)	7.7	7.7
L-Valine (g/kg)	11.6	11.6
Taurine (g/kg)	0.3	0.3
Cellulose (g/kg)	50.0	50.0
Mineral mix (79055) (g/kg)	13.4	13.4
Calcium phosphate (g/kg)	21.8	21.8
Calcium carbonate (g/kg)	8.3	8.3
Vitamin Mix (40060)	10.0	10.0

Table S3. Primers used for qPCR analyses.

Gene	Forward primer	Reverse primer
Mus musculus		
Alanine-glyoxylate aminotransferase (*Agxt1*)	AAGGCATCCAGTATGTGTTCCA	TTCCGGTTAGAAAGGAGTCCC
Alanine-glyoxylate aminotransferase 2 (*Agxt2*)	TCACCTGAGAAATACCAGTCCC	CAAAGAGCCACTCCATGTGTC
Serine hydroxy-methyltransferase 1 (*Shmt1*)	GGATGATAATGGGGCGTATCTCA	GTCTTGTGGGTTGTAGTGGTC
Serine hydroxy-methyltransferase 2 (*Shmt2*)	ATGCCCTATAAGCTCAATCCCC	TCTCATGCGTGCATAGTCAATG
Choline dehydrogenase (*Chdh*)	TGAGCTGGGTGCCAATATGTA	CGAAGCCCTCCTGTTGGAA
Sarcosine dehydrogenase (*Sardh*)	GAGAGCGACTGACCTCTGG	CCGTGTGTGAGCCAAAAGC
Threonine dehydrogenase (*Tdh*)	CTGGCTGTTTCACTACAGTGC	GGAGAGGTAGGTCCAAAGGC
Peroxisome proliferator activated receptor alpha (*Ppara*)	AACATCGAGTGTCGAATATGTGG	CCGAATAGTTCGCCGAAAGAA
Acyl-Coenzyme A oxidase 1 (*Acox1*)	CCGCCACCTTCAATCCAGAG	CAAGTTCTCGATTTCTCGACGG
Hydroxyacyl-Coenzyme A dehydrogenase alpha (*Hadha*)	ACCTCGGTGTAAAGCACAAAGT	GAGGTTTTGTCAGTGGTGATGA
Acetyl-Coenzyme A acyltransferase 2 (*Acaa2*)	AGTCCCCCTACTGTGTCAGAAA	CCATCTCCTCATTGAAGTAGCC
Enoyl-Coenzyme A delta isomerase 1 (*Eci1*)	TGCTGTGACTACAGGGTTATGG	GATCCTCAGGTACCACCTCATC
Enoyl-Coenzyme A delta isomerase 2 (*Eci2*)	ACTACTGCAGTGGGAATGACCT	ATAGTCCCAGAAGGGTGACAGA
Acyl-CoA Synthetase Long Chain 1 (*Acsl1*)	GAGCAATGATCACTCACCAAAA	TCTTAGCTCCATGACACAGCAT

Acyl-CoA thioesterase 3 (*Acot3*)	GCTCAGTCACCCTCAGGTAA	AAGTTTCCGCCGATGTTGGA
Acyl-CoA thioesterase 4 (*Acot4*)	ACATCCAAAGGTAAAAGGCCCA	TCCACTGAATGCAGAGCCATT
Nudix-type motif 19 (*Nudt19*)	GCACCACCACAGTTCTATGAAA	TAAGGACTTTGCCTTCCTTCAC
Acyl-CoA synthetase medium-chain 5 (*Acsm5*)	TGACAGCGAAGGATCTCAAGTA	GAGTTCTCGGAAATTGATCCAG
Nuclear factor of kappa light polypeptide gene enhancer in B cells 1, p105 (*Nfkb1*)	GGTATGGCTACTCGAACTACGG	TTTCCTTCTCAGGGAGAGTCAG
Nuclear factor of kappa light polypeptide gene enhancer in B cells 2, p49/p100 (*Nfkb2*)	GAGGTTCGGTTCTATGAGGATG	CTCTGCACTTCCTCCTTGTCTT
Avian reticuloendotheliosis viral (v-rel) oncogene related B (*Relb*)	ATCCTCTCTGAGCCTGTCTACG	CACATCAGCTTGAGAGAAGTCG
Tumor necrosis factor (*Tnf*)	CTGTGAAGGGAATGGGTGTT	GGTCACTGTCCCAGCATCTT
Tumor necrosis factor receptor superfamily 9 (*Tnfrsf9*)	GTTTTGCTCCTCTACCCACAAC	CTTAAGCACAGACCTTCCGTCT
C-C motif chemokine ligand 2 (*Ccl2*)	TTAAAAACCTGGATCGGAACCAA	GCATTAGCTTCAGATTTACGGGT
C-C motif chemokine ligand 5 (*Ccl5*)	ATATGGCTCGGACACCACTC	CCACTTCTTCTCTGGGTTGG
C-C motif chemokine receptor 2 (*Ccr2*)	GATGATGGTGAGCCTTGTCATA	AGTGAGCCCAGAATGGTAATGT
C-C motif chemokine receptor 5 (*Ccr5*)	ACCCTGTCATCTATGCCTTTGT	GTGGATCGGGTATAGACTGAGC
Toll-like receptor 2 (*Tlr2*)	CGGCTGCAAGAGCTCTATATTT	TGGCGTCTCCATAGTAAAGGAT
Toll-like receptor 4 (*Tlr4*)	CAGCACTCTTGATTGCAGTTTC	CATTCACCAAGAACTGCTTCTG
CD86 Antigen (*Cd86*)	TCTTGCTGATCTCAGATGCTGT	CGTACAGAACCAACTTTTGCTG

Transforming growth factor, beta 1 (*Tgfb1*)	TGCGCTTGCAGAGATTAAAA	CTGCCGTACAACTCCAGTGA
Transforming growth factor, beta 2 (*Tgfb2*)	CTAATGTTGTTGCCCTCCTACAG	GCACAGAAGTTAGCATTGTACCC
Transforming growth factor, beta receptor 1 (*Tgfbr1*)	GGACCATTGTGTTACAAGAAAGC	CATGGCGTAACATTACAGTCTGA
Transforming growth factor, beta receptor 2 (*Tgfbr2*)	TCCTAGTGAAGAACGACTTGACC	TACCAGAGCCATGGAGTAGACAT
Collagen, type I, alpha 1 (*Col1a1*)	TGAACGTGACCAAAAACCAA	GCAGAAAAGGCAGCATTAGG
Collagen, type I, alpha 2 (*Col1a2*)	AGGCAGGTCTGGGCTTTATT	CGTATCCACAAAGCTGAGCA
Collagen, type III, alpha 1 (*Col3a1*)	CTGTGAATCATGTCCAACTGGT	GATCCAGGATGTCCAGAAGAAC
Collagen, type IV, alpha 1 (*Col4a1*)	CAGGCATAGTCAGACAACAGATG	TGGACAGCCAGTAAGAGTAGTCG
Collagen, type IV, alpha 2 (*Col4a2*)	CCCATCTGACATCACACTTGTT	CCTCTGCTTCCTTTCTGTCCTA
Tissue inhibitor of metalloproteinase 1 (*Timp1*)	ATTCAAGGCTGTGGGAAATG	CTCAGAGTACGCCAGGGAAC
Tissue inhibitor of metalloproteinase 2 (*Timp2*)	AGAAGAAGAGCCTGAACCACAG	GGTCCTCGATGTCAAGAAACTC
Serine (or cysteine) peptidase inhibitor, clade E, member 1 (*Serpine1*)	GTAGCACAGGCACTGCAAAA	ATCACTTGGCCCATGAAGAG
Peroxisome proliferative activated receptor, gamma, coactivator 1 alpha (*Ppargc1a*)	ATCACGTTCAAGGTCACCCTAC	TTCTGCTTCTGCCTCTCTCTCT
Acyl-Coenzyme A dehydrogenase, medium chain (*Acadm*)	CTGTGATTCTTGCTGGAAATGA	GCCGTTGATAACATACTCGTCA
Acyl-Coenzyme A dehydrogenase, long chain (*Acadl*)	CTATATTGCGAATTACGGCACA	ACACCTTGCTTCCATTGAGAAT

Acyl-Coenzyme A dehydrogenase, very long chain (*Acadvl*)	GCAGATGAGTGCATCCAAATAA	TGAGTTCCTTTCCTTTGTCCAT
Hydroxyacyl-Coenzyme A dehydrogenase (*Hadh*)	AACACGTCTTCTTTGCAGATCA	AATGAGGTATGGCACCAAGAGT
Cytochrome P450, family 4, subfamily a, polypeptide 14 (*Cyp4a14*)	TATGTCCTCTGATGGACGTTTG	CTGTTCCTATCCTCCATTCTGG
Mitochondrial carnitine/acylcarnitine translocase (*Cact*)	CAACCACCAAGTTTGTCTGGA	CCCTCTCTCATAAGAGTCTTCCG
Carnitine palmitoyltransferase 1a (*Cpt1a*)	AGATCAATCGGACCCTAGACAC	CAGCGAGTAGCGCATAGTCA
Patatin-like phospholipase domain containing 2 (*Pnpla2*)	TCCGTGGCTGTCTACTAAAGA	TGGGATATGATGACGTTCTCTCC
Glutathione S-transferase, theta 2 (*Gstt2*)	CTCATGTCTCTGGAGGAGTTGAT	GAGGGGGTACTGGTAACATTTTC
Glutathione S-transferase, theta 3 (*Gstt3*)	AGAGTGTGGCCATCTTGTTGTAT	AACACAGGGAACATCATCTTCTG
Glutathione peroxidase 6 (*Gpx6*)	TCTATGAGTATGGAGCCAACACC	TCTGAGTTCTTTCCAGGTTCTTG
Microsomal glutathione S-transferase 1 (*Mgst1*)	GAAGACTGAGACCAAGATTGGAA	CTTGTTGGTTATCCTCTGGAATG
Glutathione S-transferase omega 1 (*Gsto1*)	GTTCTTTGAGAAGAATCCCCTTG	TTCGGAGAGTCTTCCTTTCTCTT
Glutathione S-transferase, alpha 3 (*Gsta3*)	TTACGAAGTGATGGGAGTCTGAT	TGTACATGTCAATGATGGCTCTC
Glutathione S-transferase kappa 1 (*Gstk1*)	AGAGATTCCTCTCCTGAAGCAGT	ACCATACACGCATCCATATCTCT
N-acetyltransferase 8, (*Nat8*)	GACATCACCAAGTCCTACCTGAG	ACAACATCACTGTAACCCTGGTC

Superoxide dismutase 1 (*Sod1*)	CAGTGCAGGACCTCATTTTAATC	CCAGCATTTCCAGTCTTTGTACT
Superoxide dismutase 2 (*Sod2*)	GATGTTACAACTCAGGTCGCTCT	GGCTGTCAGCTTCTCCTTAAACT
Catalase (*Cat*)	CGATATCACCAGATACTCCAAGG	GATCCCAGTTACCATCTTCAGTG
Thioredoxin (*Txn2*)	AGACACCAGTTGTTGTGGACTTT	CACAGCTGACACCTCATATTCAA
Paraoxonase 1 (*Pon1*)	AGACACCAGTTGTTGTGGACTTT	CACAGCTGACACCTCATATTCAA
Paraoxonase 1 (*Pon2*)	GTAAACCACCCACAATTCAAGAG	TTGCCCAGTGTAGGTTCAAGTAT
Paraoxonase 1 (*Pon3*)	AAGAACAACAACGCTCTCTCATC	ACCTCTTTTGGGCTGTAGAAAAC
Peroxiredoxin 4 (*Prdx4*)	TCTCAGAGTGGTTGACTCTCTCC	CTGGGGTGTATAACGGAGGTATT
Peroxiredoxin 6 (*Prdx6*)	AAGGATTCCACTTCTTTCTGACC	TCTTCTCCATGCTTGTCAGTGTA
Glyceraldehyde-3-phosphate dehydrogenase (*Gapdh*)	CTGCGACTTCAACAGCAACT	GAGTTGGGATAGGGCCTCTC
Homo sapiens		
Alanine-glyoxylate aminotransferase (*AGXT1*)	AGAGACATCGTCAGCTACGTCA	CAGGTCACAGCTTCTTCTTGG
Glyceraldehyde-3-phosphate dehydrogenase (*GAPDH*)	ACAACTTTGGTATCGTGGAAGG	GCCATCACGCCACAGTTTC